OXFORD UNIVERSITY PRESS | Brain

# Phospholipase A2 activating protein is associated with a novel form of Leukoencephalopathy

|  | Chopra, Ashok; University of Texas Medical Branch at Galveston |
|---|---|
| Subject category: | Genetics |
| To search keyword list, use whole or part words followed by an *: | Genetics: neurodegeneration < GENETICS, Transgenic model < GENETICS, Whole-exome sequencing < GENETICS, Spasticity < MOVEMENT DISORDERS, Brain development < SYSTEMS/DEVELOPMENT/PHYSIOLOGY |
|  |  |

SCHOLARONE™
Manuscripts

1    **Phospholipase A$_2$-activating protein is associated with a novel form of**

2    **leukoencephalopathy**

3    Tzipora C. Falik Zaccai MD[1,2], David Savitzki MD[3]*, Yifat Zivony-Elboum PhD[1]*,

4    Thierry Vilboux PhD[4,5]*, Eric C. Fitts PhD[6]*, Yishay Shoval PhD[1], Limor Kalfon

5    PhD[1], Nadra Samra MD[1], Zohar Keren PhD[1], Bella Gross MD[2,7], Natalia Chasnyk

6    MD[1], Rachel Straussberg MD[8,9], James C Mullikin PhD[10,11], Jamie K. Teer PhD[12],

7    Dan Geiger PhD[13], Daniel Kornitzer PhD[14] Ora Bitterman-Deutsch MD[2,15], Abraham

8    O. Samson PhD[2], Maki Wakamiya PhD[16], Johnny W. Peterson PhD[6], Michelle L.

9    Kirtley[6], Iryna V. Pinchuk, PhD[17], Wallace B. Baze DVM, PhD[18],William A Gahl

10   MD PhD[4], Robert Kleta MD PhD[19], Yair Anikster MD PhD[9,20] , Ashok K. Chopra

11   PhD, CSc[6]

12   [1]Institute of Human Genetics, Galilee Medical Center, Nahariya, Israel

13   [2] Faculty of Medicine in the Galilee, Bar Ilan University, Safed, Israel

14   [3]Pediatric Neurology Unit, Galilee Medical Center, Nahariya, Israel

15   [4]Section on Human Biochemical Genetics, Medical Genetics Branch, National Human

16   Genome Research Institute, National Institutes of Health, Bethesda, MD, USA

17   [5]Division of Medical Genomics, Inova Translational Medicine Institute, Inova Health

18   System, Falls Church, VA, USA

19   [6]Department of Microbiology & Immunology, University of Texas Medical Branch,

20   Galveston, TX, USA

21   [7]Department of Neurology, Galilee Medical Center, Nahariya, Israel

22   [8]Pediatric Neurology Unit, Schneider Children's Medical Center, Petach Tikva, Israel

23   [9]Sackler School of Medicine, Tel Aviv University, Tel Aviv, Israel

24   [10]Comparative Genomics Analysis Unit, National Human Genome Research Institute,

25   National Institutes of Health, Bethesda, MD, USA

1   [11]NIH Intramural Sequencing Center, National Human Genome Research Institute,

2   Rockville, MD, USA

3   [12]Dept. of Biostatistics and Bioinformatics, H. Lee Moffitt Cancer Center, Tampa, FL,

4   USA

5   [13]Computer Sciences, Technion - Israel Institute of Technology, Haifa, Israel

6   [14]Faculty of Medicine, Technion - I.I.T. and Rappaport Institute for Biomedical

7   Research, Haifa, Israel

8   [15] Dermatology Clinic, Galilee Medical Center, Nahariya, Israel

9   [16]Transgenic Mouse Core Facility, Institute for Translational Sciences and Animal

10  Resource Center, University of Texas Medical Branch, Galveston, TX, USA

11  [17]Department of Internal Medicine, University of Texas Medical Branch, Galveston,

12  TX, USA

13  [18]Department of Veterinary Sciences, MD Anderson Cancer Center, Bastrop, TX,

14  USA

15  [19]University College, Royal Free Hospital / UCL Medical School, London, UK

16  [20]Metabolic Disease Unit, Edmond and Lily Safra Children's Hospital, Sheba Medical

17  Center, Tel Aviv, Israel.

18  *These authors contributed equally to this paper.

19  **Running head**: PLAA and progressive leukoencephalopathy

20  **Corresponding author:** Tzipora C. Falik-Zaccai, MD

21  Institute of Human Genetics, Galilee Medical Center

22  P.O. Box 21, Nahariya 22100. Israel

23  Tel: 972-50-7887-941; Fax: 972-4-9107553*; E-mail: falikmd.genetics@gmail.com*

1   **Abstract**

2   Leukoencephalopathies are a group of white matter disorders related to abnormal

3   formation, maintenance, and turnover of myelin in the central nervous system. These

4   disorders of the brain are categorized according to neuroradiological and

5   pathophysiological criteria. Herein, we have identified a unique form of

6   leukoencephalopathy in seven patients presenting at ages two to four months with

7   progressive microcephaly, spastic quadriparesis, and global developmental delay.

8   Clinical, metabolic, and imaging characterization of seven patients followed by

9   homozygosity mapping and linkage analysis were performed. Next generation

10  sequencing, bioinformatics, and segregation analyses followed, to determine a loss of

11  function sequence variation in the phospholipase $A_2$-activating protein encoding gene.

12  Expression and functional studies of the encoded protein were performed and

13  included measurement of prostaglandin E2 and cytosolic phospholipase $A_2$ activity in

14  membrane fractions of fibroblasts derived from patients and healthy controls.

15  phospholipase $A_2$-activating protein -null mice were generated and prostaglandin $E_2$

16  levels were measured in different tissues. The novel phenotype of our patients

17  segregated with a homozygous loss of function sequence variant, causing the

18  substitution of Leucine at position 752 to Phenylalanine, in the phospholipase $A_2$-

19  activating protein, which causes disruption of the protein's ability to induce

20  prostaglandin $E_2$ and cytosolic phospholipase $A_2$ synthesis in patients' fibroblasts.

21  *Plaa*-null mice were perinatal lethal with reduced brain levels of prostaglandin $E_2$.

22  The non-functional phospholipase $A_2$-activating protein and the associated

23  neurological phenotype, reported herein for the first time, join other complex

24  phospholipid defects that cause leukoencephalopathies in humans, emphasizing the

25  importance of this axis in white matter development and maintenance.

1    **Keywords:** Phospholipase $A_2$-activating protein; progressive leukoencephalopathy;

2    autosomal recessive; startle response; complex phospholipid defects

3

1    **Introduction**

2    Leukoencephalopathies are brain white matter disorders categorized by

3    neuroradiological and pathophysiological criteria (van der Knaap, 2001) into:

4    (a) Hypomyelinating diseases that are primary disturbances in myelin formation;

5    Pelizaeus-Merzbacher disease  may be considered the prototype of hypomyelinating

6    disorders. Additionally, Pelizaeus-Merzbacher-like diseases phenotypically resemble

7    Pelizaeus-Merzbacher disease but are inherited as autosomal-recessive disorders.

8    Typically, no gene is identified, but in a small subset of Pelizaeus-Merzbacher-like

9    diseases patients, sequence variations in *gap junction protein alpha 12*, coding for

10   connexin 46.6 (Henneke et al., 2008; Uhlenberg et al., 2004), and sequence variations

11   in the gene *HSPD1,* coding for heat shock 60-kDa protein 1, have been found (Magen

12   *et al*., 2008). This group also includes syndromes in which hypomyelination is

13   accompanied by other multi-organ involvements such as Cockayne's and

14   Trichothiodystrophy Syndromes (Weidenheim *et al.*, 2009), and Oculodentodigital

15   Dysplasia and 4H Syndrome (Atrouni *et al.*, 2003; Timmons *et al*., 2006).

16    (b) Dysmyelinating disorders with delayed and disturbed myelination, including most

17   amino-acidopathies and organic acidurias. Since the brain (especially glial cells) is

18   very sensitive to accumulation of toxic metabolites, secondary white matter

19   abnormalities can be diagnosed in many metabolic disorders. Dysmyelination is also a

20   main pattern of rare disorders such as SOX10-Associated Syndromes (the neurologic

21   variant of Waardenburg-Shah Syndrome) (Pusch *et al*., 1998). Affected patients

22   present a variable range of neurological symptoms: developmental delay, spasticity,

23   ataxia, nystagmus, and in severe cases, profound neonatal hypotonia and congenital

24   arthrogryposis due to peripheral hypomyelination. 18q Deletion Syndrome, another

25   example for disorders in this category, is characterized by neurological features such

1    as mental retardation, microcephaly, hypotonia, nystagmus and seizures, accompanied

2    by additional multisystem defects, including partial growth hormone deficiency,

3    facial, external ear, cardiac, and skeletal defects. Regions for dysmyelination,

4    congenital aural atresia, and growth hormone insufficiency (18q22.3-q23) were

5    identical and contained 5 known genes, including the myelin basic protein encoding

6    gene. The dysmyelination region was 100% penetrant (Feenstra *et al*., 2007).

7    (c) The third group is disorders with progressive demyelination, including "classic"

8    leukodystrophies: X-linked adrenoleukodystrophy, Alexander's disease,

9    Metachromatic leukodystrophy, Krabbe's disease, and disorders with white-matter

10    vacuolisation such as Canavan's disease and Vanishing White Matter disease.

11    (d) Several leukoencephalopathies present with cystic degenerations, including

12    megalencephalic leukoencephalopathy with subcortical cysts, first described by van

13    der Knaap *et al*. in 1995 (van der Knaap *et al.*, 1995). Early-onset macrocephaly and

14    delayed-onset neurologic deterioration, including cerebellar ataxia, spasticity,

15    epilepsy, and mild cognitive decline, are characteristic features. Cystic

16    leukoencephalopathy without megalencephaly has also been described (Henneke *et*

17    *al.,* 2009).

18     (e) Disorders secondary to axonal damage include the autosomal recessive disorder

19    giant axonal neuropathy**.**  Patients present with progressive gait disturbances due to

20    peripheral neuropathy, mental retardation, optic atrophy and spasticity; brain imaging

21    studies show leukoencephalopathy. Pathological hallmarks of giant axonal neuropathy

22    are axonal loss and axonal swellings filled with neurofilaments on nerve biopsy (Tazir

23    *et al.*, 2009). Giant axonal neuropathy is caused by sequence variation in *GAN*

24    encoding for gigaxonin, located on chromosome 16q24 (Bomont *et al.,* 2000).

1    Nevertheless, 50% of patients with leukoencephalopathies remain without specific

2    diagnosis.

3    We report seven individuals from two consanguineous families presenting a unique

4    phenotype of severe spastic quadriparesis, progressive microcephaly, thin corpus

5    callosum, significant startle response, and severe global developmental delay. Genetic

6    investigation revealed a novel missense variant in the phospholipase $A_2$-activating

7    protein (*PLAA*) gene and disclosed a new mechanism required for normal

8    development and maintenance of central nervous system white matter.

9    **Methods**

10   **Patients**

11   The Israeli Ministry of Health Ethics Committee for genetic experiments approved

12   the proposed studies. Seven affected and twenty-three healthy individuals from two

13   consanguineous families were enrolled in the study; they or their legal guardians

14   provided written, informed consent. Clinical investigations included medical

15   procedures, imaging and electrophysiological studies, and muscle biopsies. Skin

16   biopsy was performed as part of the research protocol.

17   **Molecular studies**

18   *Genetic Linkage Analysis*

19   Linkage and haplotype analyses were performed as previously described (Zivony-

20   Elboum *et al.*, 2012).

21   An analysis of 2050 polymorphic markers, spread across the genome at approximately

22   2cM intervals was performed for 9 family members. Statistical analysis of the

23   logarithm of the odds (LOD) score was performed using the Pedtool-superlink tool.

24   Areas with high LOD score were further examined using Linkage Mapping Set v2.5

1    HD5 kit and v2.5 MD10 (Applied Biosystems, Grand Island, NY) on 24 family

2    members, according to the manufacturer's protocol.

3    *Molecular Inversion Probes and Massively Parallel Sequencing*

4    Molecular Inversion Probes were designed as described (Teer *et al.*, 2010) to cover

5    the 2Mb of the candidate region (LC Sciences, Houston, TX). A total of 6498

6    amplimers had an average length of 433bp (+/-22bp). The amplimers covered 97% of

7    the candidate region. DNA capture, library preparation, GAIIx sequencing (Illumina,

8    San Diego, CA), and data analysis were performed as described (Teer *et al.*, 2010).

9    Potential variants were filtered and visualized with VarSifter (Teer *et al*., 2012).

10    *Sanger Sequencing*

11    For dideoxy sequencing, primers were designed to cover the candidate sequence

12    variations (primer sequences available upon request). Direct sequencing of the

13    polymerase chain reaction (PCR) amplification products was performed using BigDye

14    3.1 Terminator chemistry (Applied Biosystems) and separated on an ABI 3130xl

15    genetic analyzer (Applied Biosystems). Data were evaluated using Sequencher v5.0

16    software (Gene Codes Corporation, Ann Arbor, MI).

17    *Molecular Modeling*

18    Molecular modeling of the PLAA protein and assessment of the sequence variation

19    impact was performed using the PyMOL Molecular Graphics System (Schrödinger,

20    New York, NY) (Baugh *et al.,* 2011).

21    **Expression analyses**

22    *Reverse Transcription of Full-Length PLAA Transcript*

23    Primary fibroblasts [from healthy controls (n*PLAA*) and patients (m*PLAA*)] were

24    harvested from one near-confluent 25 cm$^2$ flask and RNA extracted using the RNeasy

25    mini kit (Qiagen, Valencia, CA). RNA samples were quantified using a Nanodrop

8

1  Spectrophotometer (Nanodrop Technologies, Wilmington, DE) and qualified by

2  analysis on an RNA NanoChip using the Agilent 2100 Bioanalyzer (Agilent

3  Technologies, Santa Clara, CA). Synthesis of complimentary DNA (cDNA) was

4  performed using the Taqman Reverse Transcription Reagents Kit (Applied

5  Biosystems). The reaction conditions were as follow: 10 min at 25ºC; 30 min at 48ºC;

6  and 5 min at 95ºC. PCR amplifications of cDNA were performed using FailSafe

7  buffer C (Epicenter Biotechnologies, Madison, WI) with *PLAA* primers

8  5'CGAGCGGCGCAACCAGGTACC3' and

9  5'GCATTCACTTACTTTAGCTGGTTCTG3' at a final concentration of 1 μM.

10  Thermal conditions for 40 cycles of PCR were as follow: 94ºC for 30 sec, 60ºC for 30

11  sec, and 68ºC for 7 min.

12  *Real Time (RT)-quantitative (q)PCR*

13  One μg of RNA extracted from fibroblasts from healthy controls and patients was

14  subjected to cDNA synthesis followed by RT-qPCR using the iTaq Universal SYBR

15  Green mix (Bio-Rad, Hercules, CA).  The final concentration of the *PLAA* primers

16  (5'GACT TGGGAATCCC AGCTTTTC3' and

17  5'TTCCCATACTTGCAGAACCTG3'; Accession # NM_001031689) was 300 nM.

18  RT-qPCR assays were performed with human 18S RNA, glyceraldehyde 3-phosphate

19  dehydrogenase (GAPDH), L19 ribosomal protein, and polymerase beta (PolB) as

20  housekeeping protein encoding genes to normalize *PLAA* transcript levels.  Absolute

21  analysis was performed using known amounts of a synthetic transcript of the gene of

22  interest.  All RT-qPCR assays were run on the ABI Prism 7500 Sequence Detection

23  System and the conditions were as follow: 50ºC for 2 min, 95ºC for 10 min, and then

24  40 cycles of 95ºC for 15 sec and 60ºC for 1 min. The results shown were the averages

25  and standard deviations from three independent experiments performed in triplicate.

9

1

2   The pro-inflammatory gene expression in fibroblasts with n*PLAA* or the m*PLAA* gene

3   was carried out using the appropriate assays-on-demand^TM gene expression assay mix

4   consisting of a 20X mix of unlabeled PCR primers and TaqMan® MGB probe,

5   FAMTM dye-labeled (Life Science Technology Inc, CA).  Human GADPH, β-actin,

6   and 18S RNA encoding genes were used to normalize transcripts for various

7   cytokines. The primer sequences for various cytokine genes are available upon

8   request. The reactions were carried out according to the manufacturer's instruction

9   using a Bio-Rad Q5 RT-qPCR machine. The results shown were the averages and

10  standard deviations from three independent experiments performed in triplicate.

11  *Western blot analysis*

12  *β-catenin.* Briefly, 70 µg of protein samples from healthy controls' and patients'

13  fibroblasts with or without lipopolysaccharide [LPS; 10 µg/mL] stimulation) were

14  electrophoresed on 4-20% Mini-Protean TGX Pre-cast Tris/Glycine gels (Bio-Rad)

15  and then transferred to nitrocellulose membranes.  The membranes were probed with

16  non-phospho (active) β-catenin (Cell Signaling Technology, Danvers, MA) and β-

17  Tubulin (Santa Cruz) antibodies as described by the manufacturer.  An anti-rabbit

18  horseradish peroxidase conjugated secondary antibody (Southern Biotech,

19  Birmingham, AL) was then added, and proteins detected by using enhanced

20  chemiluminescence with Super Signal West Femto Maximum Sensitivity substrate

21  (Thermo Scientific).  The membranes were then imaged with GE ImageQuant LAS

22  4000 (General Electric, Fairfield, CT).

23  **Biochemical studies**

24  *Measurement of Prostaglandin E2 (PGE$_2$)*

1   Primary human fibroblasts from healthy controls and patients were grown in Dulbecco

2   modified essential medium with 15% fetal bovine serum at 37°C and 5% $CO_2$.

3   Fibroblasts from patients and control subjects were treated with 10 μg/mL LPS or

4   cholera toxin for 24 hours; and the cell culture supernatants were collected. $PGE_2$

5   levels were determined using enzyme immunoassay kit (Cayman Chemicals, Ann

6   Arbor, MI). To examine $PGE_2$ levels in mouse tissues, samples were subjected to

7   solid phase extraction on $C_{18}$ columns (Cayman Chemicals) prior to measurements.

8   *Preparation of Membrane Fractions from Fibroblasts*

9   Membrane fractions from healthy controls and patients' unstimulated and LPS-

10  stimulated fibroblasts were isolated using established procedures (Zhang *et al.,* 2008).

11  Protein concentrations in membrane fractions were determined using Bradford Protein

12  Reagent (Bio-Rad).

13  *Measurement of Cytosolic Phospholipase $A_2$ (cPLA$_2$) Activity*

14  The cPLA$_2$ activity in membrane fractions of fibroblasts from patients and healthy

15  controls) was determined using PLA$_2$ activity kit (Cayman Chemicals). The

16  enzymatic activity was normalized to protein concentration for each sample. Bee

17  Venom PLA$_2$ was used as a positive control.

18  *Complementation studies*

19  Fibroblasts from patients (*mPLAA*) or healthy controls (*nPLAA*) were grown and

20  electroporated with the recombinant plasmid or the vector alone using Lonza

21  Nucleofector and Human Dermal Fibroblast kit (Lonza, Basel, Switzerland). The

22  m*PLAA* fibroblasts were electroporated with either CMV promoter-based pIRES2-

23  DsRed2-*nPLAA* for complementation or pIRES2-DsRed2 vector (Clontech, Mountain

24  View, CA) alone as a control. n*PLAA* fibroblasts were also electroporated with the

25  vector alone to serve as an additional control.

1    **Mouse model**

2    All animal experiments were performed at the University of Texas Medical Branch.

3    Animals were housed in a specific-pathogen free facility at a constant temperature

4    (68-79$^o$F) and humidity (30-70%) on a 12 hours light-dark cycle. Autoclaved water

5    and irradiated feed were given to the animals *ad libitum*. All procedures were

6    performed in accordance with the protocol reviewed and approved by University of

7    Texas Medical Branch Institutional Animal Care and Use Committee, and in

8    compliance with the institutional policies/guidelines and the Guide for the Care and

9    Use of Laboratory Animals, 8$^{th}$ edition.  Euthanasia methods used in the procedures

10   were consistent with the American Veterinary Medical Association Guidelines for the

11   Euthanasia of Animals, 2013 edition.  Generation of *Plaa*-null mice (*Plaa* gene

12   targeting) and genotyping of the mice have been described in Supplemetary Materials

13   and Methods section.

14   *Preparation of Mouse Tissue Samples for PGE$_2$ Measurements*

15   In brief, mouse tissues were suspended in homogenization buffer (0.1M disodium

16   phosphate buffer, pH 7.4, 1 mM EDTA, 10 µM indomethacin) and sonicated.

17   Samples were normalized by measuring protein concentrations using the Bradford

18   Protein Reagent (Bio-Rad). After homogenization, 4 volumes of ethanol were added

19   and samples centrifuged at 3000 x *g* for 10 min at 4°C. Supernatants were collected

20   and ethanol removed by vacuum centrifugation before acidification of the samples

21   with 1M acetate buffer. The samples were then loaded on pre-washed C$_{18}$ cartridges,

22   washed with H$_2$O, and eluted with ethyl acetate and 1% methanol (99:1 v/v). Ethyl

23   acetate was removed by vacuum centrifugation and samples reconstituted in PGE$_2$

24   assay buffer for measuring PGE$_2$.

25   **Histopathology**

1    Sections (5 µm) representing skin, lungs, and the brain cerebral cortex from

2    embryonic day (E) 18.5 mouse embryos were fixed in 10% neutral buffered formalin.

3    The tissue sections were mounted on slides and stained with hematoxylin and eosin.

4    The histopathological evaluation of the tissue sections was performed in a blinded

5    fashion.

6    **Statistical analysis**

7    Where appropriate, at least three independent experiments were performed in

8    triplicate and data analyzed using one-way ANOVA with Tukey or Tukey *post-hoc*

9    correction.

10

1    **Results**

2    **Patients**

3    Seven individuals from two families, all products of consanguineous marriages and

4    uneventful pregnancies, presented with progressive leukoencephalopathy (**Figure**

5    **1A&B**), defined as dysmyelinating according to the known categories of Van der

6    Knaap and his colleagues (van der Knaap, 2001). Affected individuals were normal at

7    birth, with onset of neurological symptoms at age 2-4 months (**Table 1**). Symptoms

8    included spasticity of lower limbs rapidly progressing to upper extremities, resulting

9    in severe quadriparesis with symptoms of corticospinal tract impairment and posture

10   deformation. Involvement of extrapyramidal system function included dystonic

11   posturing, rigidity/freezing, and hypomimia/amimia. All patients suffered from severe

12   mental and language developmental delay. The motor functions were also

13   prominently impaired (level V, according to Gross Motor Function Classification

14   System (Palisano et al., 1997). Abnormally exaggerated startle reflex to an auditory

15   stimulus was observed in 6 patients, and seizures developed in three.

16   Head circumferences, normal at birth, decreased to more than 2 standard deviation

17   below the mean in the ensuing years. In two patients, we observed an unexplained

18   gradual increase in Head circumferences  up to 75% after the age of approximately 5

19   years. Weight and height, also normal at birth, fell to 3-4 SD below mean in 5 patients

20   but returned to 50-75% in two out of five patients. Progressive chest deformities

21   (kyphosis/pectus carinatum) were observed in all patients. Additional phenotypic

22   characteristics included contractures of large joints, hyperextensibility of small ones,

23   rocker bottom feet, hypertrichosis, and hyperhidrosis of palms and feet (**Figure 1C, a-**

24   **d**).

1    Brain MRI demonstrated radiological signs of periventricular and subcortical damage

2    including delayed myelination and atrophy, which worsened with age as a result of

3    enlargement of ventricular system. Thin corpus callosum was a prominent feature in

4    all of the patients. In one case, periventricular lesions were observed (Figure 1D).

5    Muscle biopsy in patient $VI_3$ showed normal oxidative phosphorylation and increased

6    aggregation of collagen.

7    **Molecular analyses**

8    *Molecular Studies*

9    Linkage analysis, performed on 24 individuals from family I, identified a 1.9Mb

10   region between markers D9S265 and rs1330920 with a maximal LOD score of 3.24 at

11   D9S1121; the region contained 11 genes (**Figure 2A&B**). Seven samples were

12   sequenced (two affected, 2 obligate carriers, and 3 unaffected individuals from the

13   same village) with an average coverage of $82 \pm 2\%$ (all coding regions were covered).

14   Haplotype analysis (D9S259-D9S169) supported a common ancestral haplotype in

15   families A and B (**Table S1).**

16   *Next Generation Sequencing*

17   A total of 4289 variants were identified, but only four of them affected protein

18   sequences (**Table S2**). Out of these four variants, only one was present in a

19   homozygous state in the affected individuals and in a heterozygous state in the

20   obligate carriers. The three others were identified in the samples of unaffected

21   individuals. The missense variant, NM_001031689.2: c.2254C>T (p.Leu752Phe); was

22   confirmed by Sanger sequencing (**Figure 2C**) in all affected individuals and obligate

23   carriers. All seven affected individuals were homozygous for this sequence variation;

24   all their parents were heterozygous.

15

1   The above PLAA variant (p.Leu752Phe) was neither observed in the Exome

2   Aggregation Consortium (60.706 unrelated individuals, Exome Aggregation

3   Consortium [ExAC], Cambridge, MA, http://exac.broadinstitute.org/, accessed

4   February 2016) nor in the NHLBI database (6,500 unrelated individuals, Exome

5   Variant Server, NHLBI GO Exome Sequencing Project, Seattle, WA [URL:

6   http://evs.gs.washington.edu/EVS/] accessed February 2016). Population screening of

7   92 healthy village residents revealed 3 carriers of this sequence variation (prevalence

8   3.3%).

9   The leucine at position 752 in PLAA is highly conserved through *Saccharomyces*

10  *cerevisiae* (**Figure 2D**), with the exclusion of Zebrafish (threonine) and

11  *Caenorhabditis elegans* (valine). This amino acid substitution is predicted to be

12  deleterious by SIFT (Score: 0.04)

13  (http://sift.jcvi.org/www/SIFT_aligned_seqs_submit.html) and probably damaging by

14  PolyPhen-2 (Score 0.983) (http://genetics.bwh.harvard.edu/pph2/index.shtml).

15  *Structural Effects of p.Leu752Phe substitution in* PLAA

16  The structure of PLAA PUL domain, in which Leu752 resides, was recently

17  determined with atomic resolution (Qiu *et al.*, 2010). PUL domain consists of 15

18  tightly packed α-helices forming a 6-mer Armadillo domain. This protein fold consists

19  of tightly packed helices in a single rigid structure found in several proteins such as

20  importin-α, β-catenins, and Hsp70 binding protein (Hatzfeld, 1999). The Armadillo

21  domain of PLAA is held together mainly through conserved leucine residues that zip

22  together adjacent α-helices. On average, leucine is present every 3-4 residues,

23  corresponding to one turn of the helical wheel. Such Armadillo repeats form banana-

24  shaped domains that generate good binding surfaces, particularly on the inside

25  curvature (Hatzfeld, 1999).

1    In PLAA, the putative binding site is also paved with conserved residue  (Sievers *et*

2    *al.*, 2011). Based on these data, p.Leu752Phe mutation appears to disrupt the tightly

3    packed leucine network of the PLAA PUL domain and deform the banana-like

4    binding surface (**Figure 2E**).

5    **Expression studies**

6    *PLAA mRNA Expression*

7    At the transcriptional level, fibroblasts from patients were capable of expressing full

8    length *PLAA* transcript similar to that of n*PLAA* fibroblasts (**Figure 3A**). Furthermore,

9    based on RT-qPCR, no difference in the levels of *PLAA* transcript was noted between

10   n*PLAA* versus m*PLAA* fibroblasts (**Figure 3B**). As amino acid changes can have

11   unexpected effects on protein stability, we sought to confirm production of PLAA

12   protein in fibroblasts with and without the defined mutation in the *PLAA* gene.

13   Confocal microscopy was performed to localize PLAA in normal and patient

14   fibroblasts. All patient fibroblasts tested showed some localization of PLAA in the

15   nucleus and majority of PLAA in the cytoplasm, which were similar in levels found in

16   the fibroblasts of healthy controls (**Figure 3C&D**).

17   *Functional Effects of p.Leu752Phe on* PLAA

18   Previous studies showed that PLAA loss causes severe ubiquitin depletion,

19   accumulation of misfolded proteins, and impaired cellular survival, in *S. cerevisiae*

20   (Mullally et al., 2006; Qiu et al., 2010). However, these effets were neither shown in

21   the growth *of S. cerevisiae* and its Δ*DOA1* (an ortholog of human *PLAA* in yeast)

22   mutant nor on ubiquitin depletion in fibroblasts from healthy controls versus patients.

23   (See methods and results in the supplementary section.) Consequently, we examined

24   other known functions of the PLAA protein. PLAA induces $PGE_2$ production by

1    increasing levels of $PLA_2$ and cyclooxygenase (COX)-2 proteins, two major

2    regulators of prostaglandins (Calignano *et al.*, 1991; Zhang *et al.*, 2008).

3    Investigating this function, we measured $PGE_2$ levels in our patients' fibroblasts.

4    Healthy, unstimulated cells expressing n*PLAA* exhibited ~2-fold higher levels of

5    $PGE_2$ compared to patients' fibroblasts (**Figure 4A black bars**); this difference

6    became much more prominent after LPS and cholera toxin treatment of the cultured

7    n*PLAA* cells (~5000-fold [light gray bars] and ~1000-fold [dark gray bars],

8    respectively). LPS treatment induced $cPLA_2$ activity in normal fibroblasts, but did not

9    elicit a similar response in patients' cells (**Figure 4B**). These results suggest that

10    p.Leu752Phe in PLAA abrogates its ability to induce prostaglandin biogenesis and

11    properly respond to related stresses. Finally, transfection with a plasmid expressing

12    n*PLAA* rescued $PGE_2$ levels and $cPLA_2$ activity in both untreated and LPS-stimulated

13    patients' fibroblasts (**Figure 4C&D**).

14    We previously observed that PLAA regulates NF-κB-mediated inflammatory

15    responses, and in particular inducible interleukin (IL)-6 (Zhang *et al.*, 2008). Herein,

16    we observed that p.Leu752Phe variation in PLAA abrogated expression of LPS

17    induced IL-6, IL-8, and macrophage migration inhibitory factor (MIF) expression in

18    patient fibroblasts when compared to fibroblasts from a representative healthy control

19    based on RT-qPCR (**Figure 4E-G**).

20    **Cell Biology studies**

21    *NF-κB Recruitment to the Nucleus is Unaffected by p.Leu752Phe in the PLAA.*

22    We investigated the NF-κB signaling pathway which is known to be regulated by

23    PLAA (Zhang et al., 2008) and show it is intact in both fibroblasts from patients and

24    healthy controls (Figure S1A&B). For detailed methods, results and figure see the

25    suplementary section.

1　*β-catenin wingless integration (Wnt) Signaling is Not Affected by p.Leu752Phe* PLAA

2　We investigated Wnt signaling by examining levels of non-phospho (active) β-catenin

3　in n*PLAA* versus m*PLAA* fibroblasts with and without LPS stimulation.  As shown in

4　**Figure S1C**, the levels of active β-catenin were increased after LPS stimulation to a

5　similar extent in both types of fibroblasts. Detailed results are summarized in the

6　supplimentary section.

7　**Mouse model**

8　*Inactivation of the Plaa Gene Results in Perinatal Lethality in Mice*

9　We generated *Plaa*-null mice using gene targeting technology (**Figure S2**). While

10　heterozygous (*Plaa*$^{+/-}$) mutants were viable and fertile, the homozygous (*Plaa*$^{-/-}$)

11　mutants exhibited perinatal lethality. Initially we genotyped 66 pups derived from

12　heterozygous intercrosses, typically on postnatal day 4-9.  Twenty-eight pups were

13　wild-type, thirty-eight were *Plaa*$^{+/-}$, and there was no *Plaa*$^{-/-}$ mutant. To determine

14　when the *Plaa*-null mice died, we set up timed heterozygous intercross mating and

15　examined embryos at different time points (**Table S3**). At E14.5, we recovered live,

16　overtly normal *Plaa*$^{-/-}$ embryos, which were indistinquishable from *Plaa*$^{+/-}$ or wild-

17　type littermates. At E18.5, we found mostly live (with a beating heart) but some dead

18　*Plaa*$^{-/-}$ embryos. *Plaa*$^{-/-}$ embryos were grossly normal but smaller than *Plaa*$^{+/-}$ or wild-

19　type littermates. The average body weights of live *Plaa*$^{-/-}$, *Plaa*$^{+/-}$, and wild-type

20　embryos were $0.83 \pm 0.11$ g (n=14), $1.03 \pm 0.17$ g (n=32), and $1.34 \pm 0.14$ (n=9) at

21　E18.5, respectively. While differences in weights between wild-type and *Plaa*$^{+/-}$ were

22　not statisitcally significant, weight differences between wild-type and *Plaa*$^{-/-}$

23　($\leq 0.0001$) and *Plaa*$^{-/-}$ and *Plaa*$^{+/-}$ ($\leq 0.001$) were significant by one way ANOVA with

24　Tukey *post hoc* correction.

1    Gross examination revealed that all of the near-term *Plaa^-/-* embryos had abnormal or

2    underdeveloped spleens, which were transparent/pale and smaller. Interestingly, we

3    also found one embryo with exencephaly/microcephaly among a total of 41 *Plaa^-/-*

4    embryos examined. We attempted to resuscitate some of the E18.5 embryos, but *Plaa^-*

5    *^/-* embryos could not be resuscitated. While *Plaa^+/-* and wild-type embryos reacted to

6    the pinch and started gasping for air, *Plaa^-/-* embryos did not make any voluntary or

7    involuntary movement. Subsequently, we also found five *Plaa^-/-* neonates that were

8    naturally delivered, but they were all found dead. Notably, one of the dead *Plaa^-/-*

9     neonates had posterior truncation. The dead *Plaa^-/-* neonates appeared to have no air

10   in their lungs. To date, we have not found any live *Plaa^-/-* neonate. These observations

11   suggest that *Plaa*-null mice likely died shortly before or after birth.

12   *A Tissue-Specific PGE$_2$ Reduction and Perinatal Lethality of Plaa-Null Mice*

13    To validate the results observed for the human fibroblasts carrying m*PLAA*, we

14   evaluated the levels of PGE$_2$ in wild-type, *Plaa^+/-*, and *Plaa^-/-* embryos. We isolated

15   lungs, brain, liver, and heart tissues from E18.5 embryos, and determined PGE$_2$ levels

16   for each organ individually (**Figure 5A-D**). In the brain, there was a gene copy

17   dependent reduction of PGE$_2$ with significant reduction in *Plaa^+/-* embryos compared

18   to wild-type ($p<0.001$) as well as a significant decreased level of PGE$_2$ in *Plaa^-/-*

19   compared to *Plaa^+/-* ($p<0.05$) embryos (**Figure 5B**). PGE$_2$ levels were significantly

20   decreased in *Plaa^-/-* lungs, and *Plaa^+/-* and *Plaa^-/-* hearts, but not in the liver (**Figure**

21   **5A,C&D**). It is unclear why gene copy dependent reduction of PGE$_2$ was noted in

22   some organs but not in others.

23   *Histopathological Analysis of Skin, Lungs, and Brain Cerebral Cortex of Plaa-Null*

24   *Mice*

1   <span style="color:red">As shown in **Figure 6A**, lungs from WT mice embryos exhibited the presence of</span>

2   <span style="color:red">organized alveolar spaces and thin alveolar walls. However, embryos from *Plaa$^{+/-}$* and</span>

3   <span style="color:red">*Plaa$^{-/-}$* mice showed progressively unorganized alveolar spaces and thickening of the</span>

4   <span style="color:red">alveolar walls, suggesting underdeveloped or immature lungs.</span>

5   In the brain cerebral cortex of wild type embryos, the neurons showed large nuclei

6   and were fully matured, with no indication of degeneration. No signs of apoptotic

7   bodies were noted. There were a few round dark cells that represented either

8   oligodendroglia or granular immature neurons (**Figure 6B**). The *Plaa$^{+/-}$* embryos had

9   smaller neuronal nuclei and about the same density of the round dark cells.  On the

10  contrary, *Plaa$^{-/-}$* embryos had a vast area of neurons with smaller dark-stained round

11  nuclei that could be described generally as "more granular" in type, an indication of

12  less maturity and differentiation. No significant differences were observed in the skin

13  of wild type versus mutant mouse embryos (**Figure 6C**). Typical tissue sections

14  representing multiple fields and from 2-4 embryos are shown.

15  **Discussion**

16  PLAA is a regulatory molecule implicated in modulating production of host cell

17  phospholipases (e.g., PLA$_2$) (Clark *et al.*, 1991; Ribardo *et al.*, 2002). Induction of

18  PLA$_2$ is highly regulated by mitogen-activated protein kinases and NF-κB (Zhang *et*

19  *al.*, 2008). PLA$_2$ hydrolyzes membrane phospholipids to produce arachidonic acid,

20  which is used as a substrate to produce prostaglandins and leukotrienes (eicosanoids)

21  through cyclooxygenase and lipoxygenase pathways, respectively (Ribardo *et al.*,

22  2002).

23  In this report, we present seven patients from two families with severe, unique,

24  progressive leukoencephalopathy. Based on the clinical and radiological findings,

25  these patients could be categorized into the group of primary delay in myelin

1    formation and disturbed myelination (van der Knaap, 2001). Brain biopsies were not

2    performed and histopathological data are not available to confirm or rule out our

3    clinical impression.

4    All patients are homozygous for a founder sequence variant (p.Leu752Phe) in *PLAA*.

5    that did not lead to the production of unstable transcript or protein.

6    The PLAA protein is composed of three major domains: N' terminal, multi-protein

7    complex assembly domain contains 7 WD40 repeats; central PFU domain includes a

8    ubiquitin binding region and an SH3 region; and C' terminal PUL domain consists of

9    6 Armadillo repeats and binds to valosin-containing protein, also known as Cdc48 and

10    p97 (Qiu et al., 2010). Our results suggest that the p.Leu752Phe sequence variant

11    disrupts the protein's Armadillo domain, possibly impairing cells' ability to induce

12    prostaglandin production through a non-NF-κB signaling pathway.

13    Armadillo folds such as those found in PLAA, importin-α, and β-catenins, play a role

14    in central nervous system development in *Drosophila*. Specifically, disruption of cell-

15    cell adhesion function of Armadillo results in construction defects of the axonal

16    scaffold (Loureiro and Peifer, 1998). Interestingly, a recent study suggested that

17    $PLA_2\alpha$ regulates the Wnt/β-catenin pathway (Han *et al.*, 2008), which is implicated in

18    neurogenesis, central nervous system morphogenesis, hirsutism, sweat gland

19    morphology, short tendons, and kyphosis (Haara et al., 2011 ; Joksimovic and

20    Awatramani, 2014; Toribio et al., 2010; Zhang et al., 2014).  In this pathway, β-

21    catenins transduce Wnt signals during embryonic development. Therefore, we

22    hypothesized that PLAA, which activates $PLA_2$, indirectly regulates the Wnt/β-

23    catenin pathway, accounting for the pathology seen in our patients. However, our data

24    indicate that the p.Leu752Phe in *PLAA* found in our patients did not alter Wnt

25    signaling.

1    Experimentally, activation of PLAA was recently shown to occur *via* 1α,25(OH)$_2$D3

2    binding to a specific membrane-associated receptor, Pdia3, in caveolae, regulating

3    growth zone chondrocytes (Doroudi *et al.*, 2014). These findings might explain non-

4    neurological features of progressive chest deformities (kyphosis/pectus carinatum)

5    present in affected individuals.

6    Complex phospholipid defects involving the central nernous system have received

7    much attention of late (Lamari *et al.,* 2013), providing insights into late-onset

8    neurodegenerative disease pathophysiology, such as gene *PLA2G6* encoding PLA$_2$,

9    underlying AR infantile neuroaxonal dystrophy, neurodegeneration associated with

10   brain iron accumulation, and early-onset dystonia/parkinsonism (Gregory et al., 2008;

11   Khateeb et al., 2006).

12   Furthermore, PGE$_2$ plays a dual role, both neurotoxic and neuroprotective, in the brain

13   and nervous system, a role modulated by its four receptors (Milatovic *et al.*, 2011).

14   Different binding affinities, varying cellular expression profiles, and attenuation of

15   secondary messengers of these receptors lead to intricate, and sometimes opposing,

16   signal transduction. While in Alzheimer's disease and amyotrophic lateral sclerosis it

17   plays a neurotoxic role (Bazan *et al.*, 2002), in excitotoxicity and cerebral ischemia

18   scenarios, PGE$_2$ is neuroprotective (Gregory *et al.,* 2008).  Thus, modulation of PGE$_2$

19   appears critical for neurological function. When PGE$_2$ levels are reduced by

20   deficiency of synthetic enzymes PLA$_2$ (Gregory *et al.,* 2008), COX-1 and COX-2

21   (FitzGerald, 2003) or PGE$_2$  receptor (EP1-4), neurological impairment might occur.

22   Mohri and colleagues (Mohri *et al*., 2006) have described prostaglandins as

23   neuroinflammatory molecules that heighten pathological response to demyelination in

24   twitchier mice. Similarly, the arachidonic acid pathway was shown to be modulated

25   during cuprizone neurotoxin induced-demyelination and remyelination processes

23

1    (Palumbo *et al.*, 2011). Altogether, these data support a causative relationship

2    between abnormal PLAA activity and the severe leukoencephalopathy seen in our

3    patients.

4    Of special interest is the prominent feature seen in six patients of exaggerated startle

5    response, previously linked to dysmyelination/hypomyelination disorders, such as

6    multiple sclerosis (MS).  In 1978, Mertin and Stackpoole showed that treatment with

7    essential fatty acids, including arachidonic acid, suppresses experimental autoimmune

8    encephalomyelitis in rats, and isabolished by inhibition of prostaglandin biosynthesis

9    (Mertin and Stackpoole, 1978). Additionally, decreased inhibition of startle generator

10   structure was reported to be associated with MS (Ruprecht *et al.*, 2002). The calcium-

11   independent $PLA_2$ inhibitor was also linked to reduced pre-pulse inhibition of acoustic

12   startle reflex in other studies (Lee *et al.*, 2009).

13   Multiple studies link $PGE_2$ and arachidonic acid pathways to neurodegenerative

14   disorders, but their exact roles in causing white matter disorders remain unclear. We

15   hypothesize that the prominent startle reflex dys-inhibition in our patients may be

16   related to brainstem lesions as part of the diffused axonal and myelin damage.

17   Additional interesting observation was that p.Leu752Phe substitution in PLAA results

18   inability of the patient fibroblasts to induce IL-6, IL-8, and MIF in response to the

19   NF-κB activating molecule LPS. While the pathophysiological relevance of this

20   observation is yet to be determined, an association between neurodegenerative

21   disorders and inflammatory cytokine responses has been suggested recently (Schmitz

22   et al., 2015). These cytokines are known for their pleiotropic function and are

23   implicated in activation of microglia, proliferation, migration, and homing of different

24   immune and non-immune cells. In addition, $PGE_2$ has been shown to be important

25   leading to increased production of IL-6 and IL-8(Cho et al., 2014). Thus, taken

1  together, our observation may suggest that the pathogenesis of the

2  leukoencephalopathy linked to the p.Leu752Phe subbstitution in PLAA implicates

3  inability to mount appropriate inflammatory responses during pre-/post-neonatal

4  development.

5  The phenotype of our patients, homozygous for p.Leu752Phe in *PLAA* and with

6  reduced cPLA$_2$ activity and PGE$_2$ levels, adds new insights into this axis and its role

7  in leukoencephalopathic disorders' pathogenesis.

8  Knockout mouse data provide a clue into potential disease mechanisms seen in the

9  patients described in this paper. The disturbance in prostaglandin signaling results in a

10  variety of pathological conditions. PLAA-deficient mice showed some phenotypes,

11  specifically perinatal death, immature lungs with reduced PGE$_2$, and reduced body

12  weight similar to that of *Ptgs1* (Cox-1)-*Ptgs2* (Cox-2) double knockouts (Yu *et al.,*

13  2006) and *Ptgs3* knockouts (Nakatani *et al.,* 2007). The double mutants, as well as

14  *Ptgs4* knockouts (Nguyen *et al.*, 1997) died perinatally due topatent ductus arteriosus,

15  *Ptgs3* knockouts showed perinatal death, possessed immature lungs, and PGE$_2$ levels

16  were markedly decreased in the organ. The mutants also exhibited decreased body

17  weight and skin morphological and physiological defects. Additionally, prostaglandin

18  signaling is implicated for its roles in a range of physiologicalprocesses such as cell

19  fate decision (Nissim *et al.,* 2014), cell differentiation (Li *et al.,* 2000), and

20  ciliogenesis (Jin *et al.,* 2014). The inability of *Plaa*-null mice to survive, which may

21  stem from impaired neuronal development in the brain, together with our findings that

22  PGE$_2$ levels were significantly reduced in the brain and the lung of *Plaa*-null mouse

23  embryos, raise the possibility that the pathogenesis of the condition we observed in

24  PLAA-deficient mice and in patients with a non-functional PLAA could be a

25  developmental defect caused at least partly by ineffective prostaglandin signaling.

1    Clearly, the *Plaa*-null mouse model provides an important tool to study the role of

2    PLAA in central nervous system development and maintenance. Creating *Plaa*

3    conditional knockout mice or *Plaa* knock-in mice carrying the p.Leu752Phe sequence

4    variant would enable us to perform more detailed histopathological studies of the

5    brain and thus to learn what type of leukoencephalopathy is caused by the *PLAA*

6    sequence variant described here or by PLAA deficiency. Such an animal model would

7    further contribute to the understanding of the significant role of arachidonic acid and

8    $PGE_2$ pathway in the normal development and maintenance of the brain.

9    In conclusion, we have presented a cohort of patients with progressive microcephaly

10   and leukoencephalopathy, providing the first documentation of a PLAA-related

11   disease. Although the interplay between PLAA, the abnormal production of $PGE_2$,

12   and the resultant hypo-myelination has not been thoroughly delineated, our data

13   clearly indicated an association of this axis with brain development. Supportive

14   evidence from the literature and improved understanding of the new players in this

15   pathway should lead to new therapeutic avenues for intervention in both rare

16   autosomal recessive disorders and late onset common diseases that involve reduced

17   central nervous system white matter.

18

19

20

21

22

23

24

25

5   **Author Contributions to the Study and Manuscript**

6   **Tzipora C. Falik Zaccai** initiated the project, was principal investigator, recruited the

7   patients and families, designed the experiments, and wrote the manuscript.

8   **David Savitzki** performed neurological and clinical work up on the patients and

9   followed them. He participated in preparing the manuscript.

10  **Yifat Zivony-Elboum** performed DNA linkage analyses and sequencing studies.

11  **Thierry Vilboux** performed NGS studies and expression analyses, and participated in

12  writing the manuscript.

13  **Yishay Shoval** performed sequencing studies, bioinformatics analyses, yeast studies,

14  and participated in writing the manuscript

15  **Limor Kalfon** performed sequencing studies, tissue cultures and haplotype analyses,

16  and participated in writing and editing the manuscript

17  **Nadra Samra** performed neurological and clinical work up on the patients and

18  participated in preparing the manuscript.

19  **Zohar Keren** performed sequencing studies and segregation analyses.

20  **Bella Gross** performed neurological and clinical work up on the patients and

21  participated in preparing the manuscript.

22  **Natalia Chesnik** performed neurological and clinical work up on the patients and

23  participated in preparing the manuscript.

24  **Rachel Straussberg** performed neurological and clinical follow up on the patients.

25  **James C Mullikin** participated in the NGS studies.

1    **Jamie K. Teer** participated in the NGS studies.

2    **Dan Geiger** performed the bioinformatics related to linkage analysis.

3    **Daniel Kornitzer** participated in the yeast studies.

4    **Ora Bitterman-Deutsch** participated in establishing fibroblasts tissue cultures of the

5    patients.

6    **Abraham O. Samson** participated in the bioinformatics analysis of the protein in

7    native and mutation state.

8    **William A Gahl** contributed to NGS studies, and participated in writing and editing

9    the manuscript.

10   **Robert Kleta** contributed to linkage and segregation analyses, and participated in

11   writing the manuscript.

12   **Yair Anikster** participated in NGS studies and expression analyses, and participated

13   in writing the manuscript.

14    **Eric C. Fitts** performed biochemical and microscopic studies, conducted data

15   analysis, and contributed to the writing of the manuscript

16   **Maki Wakamiya** developed and maintained transgenic mouse lines and obtained

17   mouse tissues for analysis.

18   **Johnny W. Peterson** interpreted data and participated in manuscript writing and

19   editing.

20   **Michelle L. Kirtley** helped in maintaining fibroblasts, isolating RNA, and performing

21   Western blot analysis.

22   **Iryna V. Pinchuk** performed experiments related to cytokine levels in fibroblasts and

23   wrote portion of the manuscript.

24   **Wallace B. Baze** performed histopathological studies on mouse tissues.

1    **Ashok K. Chopra** designed the experiments, interpreted the data, and participated in

2    writing and editing of the manuscript.

3    **Potential Conflicts of Interest: None**

4

5

1 **Table 1**. Clinical characteristics of patients: Data were collected regarding medical

2 history, metabolic measurements, imaging, electrophysiological studies and muscle

3 biopsy. Complete physical, neurological, and developmental examinations were

4 performed on seven patients. The disease phenotype in all patients was similarly

5 severe. NA=Not Available. MRI= Magnetic Resonance Imaging.

6 SSEP= Somatosensory Evoked Potentials.

| Patient | $A(VI_3)$ | $A(VI_4)$ | $A(VI_5)$ | $A(V_6)$ | $A(VI_{10})$ | $B(IV_2)$ | $A(VI_1)$ |
|---|---|---|---|---|---|---|---|
| Sex | F | F | M | M | M | M | M |
| Age (y) | 15 | 11 | 16 | 34 | 5 | 3 | 2 |
| AO (m) | 4 | 4 | 3 | 4 | 3 | 2 | 3 |
| FTT | +++ | + | +++ | +++ | ++ | +++ | +++ |
| Progressive microcephaly | +++ | + | +++(*) | *+ | + | +++ | + |
| Pyramidal Signs Lower extremities | +++ (plegia) Babinski sign | +++ Babinski sign | +++ Babinski sign, Clonus | +++ Babinski sign | +++ Babinski sign | ++ | +++ |
| Pyramidal Signs Upper extremities | ++ | ++ | ++ | ++ | ++ | ++ | +++ |
| Extra-pyramidal Signs | ++ | ++ | +++ | +++ | ++ | +++ | +++ |
| GMFCS (Level) | V | V | V | V | V | V | V |
| Cognitive and Language Development | Severe | Severe | Severe | Severe | Severe | Severe | Severe |

| Patient | A(VI$_3$) | A(VI$_4$) | A(VI$_5$) | A(V$_6$) | A(VI$_{10}$) | B(IV$_2$) | A(VI$_1$) |
|---|---|---|---|---|---|---|---|
| Delay | | | | | | | |
| Exaggerated Startle Response | + | + | + | NA | + | + | + |
| Seizures | - | - | + | + | - | + | - |
| MRI/CT of brain | Reduce mass of white matter. Thin Corpus Callosum Delayed Myelination (especially along Cortico-Spinal tract and posterior Genu of Capsula Interna (at age 13m) Worsening of brain atrophy at the age of 3 2/12. Sparing of basal ganglia. | Enlargement of ventricular system Thin Corpus Callosum Normal MRI of spinal cord (at age 1y) | White matter atrophy with periventricular lesions resemble PVL Thin Corpus Callosum (at age 2y) | Severe general and especially white matter atrophy and thin Corpus Callosum (at age 30y | White matter atrophy, periventricular and subcortical lesions Thin Corpus Callosum Enlargement of ventricular system (at age 1y 9m) | Delayed myelination. Thin Corpus Enlargement of ventricular system (at age 2y) | Delayed myelination (at age 9m) |
| Kyphosis/ Pectus | +/+++ | +/+++ | +/+++ | +++/+++ | +/++ | -/++ | +/+ |

| Patient | A(VI$_3$) | A(VI$_4$) | A(VI$_5$) | A(V$_6$) | A(VI$_{10}$) | B(IV$_2$) | A(VI$_1$) |
|---|---|---|---|---|---|---|---|
| Carinatum | | | | | | | |
| Hyper-trichosis | + | + | NA | + | + | - | - |
| Small joints Hyper-flexibility | + | + | ++ | - | ++ | + | + |
| Large joints Contractures | +++ Rocker bottom feet | +++ | +++ | +++ Rocker bottom feet | +++ | ++ | + |
| Intensive sweating of palms and feet | + | + | - | + | + | + | + |
| Miscellaneous | Moderate/severe hearing impairment SSEP: central bilateral disturbance in central tract conduction above brainstem. Muscle biopsy revealed sediment of | SSEP: central bilateral disturbance in central conduction above brainstem | Muscle biopsy: mild reduction of cytochrome C oxidase activity. Normal Immunohistochemical staining. Normal muscle cells structure . | | Occasional horizontal nystagmus. Retinal atrophy with abnormal VEP'S and ERG responses | | |

33

| Patient | A(VI$_3$) | A(VI$_4$) | A(VI$_5$) | A(V$_6$) | A(VI$_{10}$) | B(IV$_2$) | A(VI$_1$) |
|---|---|---|---|---|---|---|---|
|  | glycogen like material (PAS positive). EM examination confirmed accumulation of glycogen. Normal respiratory chain |  |  |  |  |  |  |

1

2    AO, age at onset; FTT, failure to thrive; GMFCS, Gross Motor Functional

3    Classification System; m, months; HC, head circumference

4    NA, not available.

5    For all of patients: normal karyotype, level of cholesterol, muscular and lysosomal

6    enzymes

7    (*) until the age of approximately 5 years followed by an unexplained gradual

8    increase in HC up to 75%.

9

10

11

12

**Figure legends**

**Figure 1. Pedigree of the investigated families**. A. Family I: 6 affected individuals (filled shapes). **B.** Family II: containing another affected individual. A high rate of consanguinity and an AR pattern of inheritance are evident. **C**. Photographs of patient $VI_5$ (pedigree A) illustrating: coarse facial features (a) pectus carinatum, dystonic posturing, rigidity/freezing and shortening of tendons (b, c), and rocker bottom feet (d).

**D.** Patients' brain MRI. a and b. T1 Brain MRI of patient $IV_2$ (family II), at 1 year of age, shows white matter atrophy. Corpus callosum is complete but thin. c (T2 MRI Imaging) and d (T1 MRI Imaging). Brain MRI of patient $VI_3$ (family I), at 14 years, shows moderate white matter atrophy and severe corpus callosum thinning. e (T2 MRI Imaging) and f (T1 MRI Imaging). Brain MRI of patient $V_4$ (family I), at age 32 years, shows severe general atrophy. The cortex is usually preserved but very thin, corpus callosum is complete but also very thin. The basal ganglia appear normal.

**Figure 2. A**. Haplotypes for each family member were constructed for 11 microsatellite markers spanning the neurodegenerative interval. Markers analyzed are given on the left, according to their physical order. Haplotypes are represented by bars, with the disease-associated haplotype shaded in gray. Reduction in the affected linked region to 1.9Mb was due to healthy individuals $VI_6$ and $IV_4$ who bear fraction of the affected haplotype in a homozygous manner.

**B**. Physical location of genes and predicted transcripts in the chromosome 9 linked interval. Asterisk denotes genes not approved by the HUGO Gene Nomenclature Committee (HGNC). "Strand" refers to transcription orientation. Bold names indicate gene analyzed by direct sequencing. Physical location obtained from UCSC Human Genome Browser Gateway (hg19 assembly).**C.** Analysis of the c.2254C>T mutation

in exon 14 of *PLAA*. Sequence analysis is shown for an unaffected individual, an

obligatory carrier, and an affected individual. **D.** Sequence alignment of human PLAA

to orthologues in the mutation area. The leucine at position 752 (*boxed*) in this protein

is highly conserved throughout evolution. **E**. Effect of L752F (Leu→Phe) substitution

on PLAA structure. Shown is a ribbon diagram of the PUL domain of PLAA (PDB ID

3EBB) which adopts a banana like shaped Armadillo domain.  The conserved

residues of PLAA (*homo sapiens*, *mus musculus*, *rattus norvegicus*, *Xenopus laevis*,

and *Saccharomyces cerevisiae*) are displayed in stick-representation and form the

putative binding site of PLAA.  Mutation of Leu752 shown in ball-representation

disrupts the rigid leucine network that tightly holds together the Armadillo domain.

**Figure 3. mRNA levels for *PLAA* and confocal microscopy of fibroblasts for the**

**presence of PLAA protein. A.** Presence of full length transcript for *PLAA* from

fibroblasts of affected patients and the control subject based on PCR. **B.** RT-qPCR for

the detection of *PLAA* transcript from fibroblasts of a patient versus the healthy

control normalized to four house-keeping genes coding for human 18S RNA,

GAPDH, PolB, and L19 ribosomal protein. Arithmetic means ± standard deviations

from three biological replicates performed in triplicate were shown. **C.** Fibroblasts

(n*PLAA* or m*PLAA*) were counterstained with DAPI (blue) for the nucleus and with

fluorophore conjugated phalloidin (red) for actin. Cells were fixed, subjected to

immunofluorescence staining for PLAA (green), and observed by confocal

microscopy. **D.** Mean fluorescence intensity of regions of interest corresponding to

the cytoplasm and nucleus of imaged cells (Image J processing program, NIH). Figure

represents results from 3 sets of images and error bars represent standard deviations.

**Figure 4. PGE$_2$ levels and cPLA$_2$ activity are low in patients' fibroblasts, and could be rescued. A.** Levels of PGE$_2$ in cell culture media after 24 hours of stimulation with LPS or cholera toxin Levels of PGE$_2$ were normalized against protein concentrations in the supernatants. All cells were primary human fibroblasts except RAW 264.7 cells which are murine macrophage like cells and used as a positive control. **B.** Activity of cPLA$_2$ in the membrane fractions of fibroblasts and RAW 264.7 macrophages. Cells were stimulated with or without LPS for 24 hours before harvesting and purification of the membrane fractions. The cPLA$_2$ activity was normalized to amount of proteins added to the assay. **C.** PGE$_2$ levels in the cell culture media after transfection with CMV promoter-based pIRES2-DsRed2 plasmid containing the native *PLAA* gene and a fluorescent marker of transfection. Cells were treated as follow: ctl = no transfection; V = transfection with empty vector; *PLAA* = transfection with plasmid vector containing the wild type *PLAA*. **D.** cPLA$_2$ activity from membrane fractions of fibroblasts after transfection with a plasmid containing the n*PLAA* in a CMV promoter-based vector system and a fluorescent marker of transfection. **E-G.** Fold changes in transcripts for IL-6, IL-8, and MIF based on RT-qPCR. Arithmetic means ± standard deviations from three independent experiments performed in triplicate were plotted and the data were analyzed using one way ANOVA with Tukey *post-hoc* correction.

**Figure 5. PGE$_2$ levels in embryonic mouse tissues.** WT, *Plaa*$^{+/-}$, and *Plaa*$^{-/-}$ embryos were sacrificed at E18.5 and organs were isolated and prostaglandin levels determined for the lung (**A**), brain (**B**), liver (**C**), and heart (**D**). Data represented arithmetic means ± standard deviations from tissues representing 3 WT, 3 *Plaa*$^{+/-}$, and 4 *Plaa*$^{-/-}$ embryos and obtained from three independent littermates. Significance was determined by one

way ANOVA with Tukey *post-hoc* correction. * denotes *p*<0.05   *** denotes

*p*<0.001.

**Figure 6.** Histopathology of embryonic mouse tissues. Lungs **(A)**, brain cerebral

cortex **(B),** <span style="color:red">and skin</span> **(C)** were H&E stained and analyzed in a blinded fashion.

Tissues representing 2 WT, 2 *Plaa*^+/-^, and 4 *Plaa*^-/-^ embryos were analyzed. Multiple

fields for each tissue were visualized and typical representations are shown with

magnifications.

References

Atrouni, S., Daraze, A., Tamraz, J., Cassia, A., Caillaud, C., Megarbane, A., 2003. Leukodystrophy associated with oligodontia in a large inbred family: fortuitous association or new entity? Am J Med Genet A. 118A, 76-81.

Baugh, E.H., Lyskov, S., Weitzner, B.D., Gray, J.J., 2011. Real-time PyMOL visualization for Rosetta and PyRosetta. PLoS One. 6, e21931.

Bazan, N.G., Colangelo, V., Lukiw, W.J., 2002. Prostaglandins and other lipid mediators in Alzheimer's disease. Prostaglandins Other Lipid Mediat. 68-69, 197-210.

Bomont, P., Cavalier, L., Blondeau, F., Ben Hamida, C., Belal, S., Tazir, M., Demir, E., Topaloglu, H., Korinthenberg, R., Tuysuz, B., Landrieu, P., Hentati, F., Koenig, M., 2000. The gene encoding gigaxonin, a new member of the cytoskeletal BTB/kelch repeat family, is mutated in giant axonal neuropathy. Nat Genet. 26, 370-4.

Calignano, A., Piomelli, D., Sacktor, T.C., Schwartz, J.H., 1991. A phospholipase A2-stimulating protein regulated by protein kinase C in Aplysia neurons. Brain Res Mol Brain Res. 9, 347-51.

Cho, J.S., Han, I.H., Lee, H.R., Lee, H.M., 2014. Prostaglandin E2 Induces IL-6 and IL-8 Production by the EP Receptors/Akt/NF-kappaB Pathways in Nasal Polyp-Derived Fibroblasts. Allergy Asthma Immunol Res. 6, 449-57.

Clark, M.A., Ozgur, L.E., Conway, T.M., Dispoto, J., Crooke, S.T., Bomalaski, J.S., 1991. Cloning of a phospholipase A2-activating protein. Proc Natl Acad Sci U S A. 88, 5418-22.

Doroudi, M., Boyan, B.D., Schwartz, Z., 2014. Rapid 1alpha,25(OH)(2)D (3)

   membrane-mediated activation of Ca(2)(+)/calmodulin-dependent protein

   kinase II in growth plate chondrocytes requires Pdia3, PLAA and caveolae.

   Connect Tissue Res. 55 Suppl 1, 125-8.

Feenstra, I., Vissers, L.E., Orsel, M., van Kessel, A.G., Brunner, H.G., Veltman, J.A.,

   van Ravenswaaij-Arts, C.M., 2007. Genotype-phenotype mapping of

   chromosome 18q deletions by high-resolution array CGH: an update of the

   phenotypic map. Am J Med Genet A. 143A, 1858-67.

FitzGerald, G.A., 2003. COX-2 and beyond: Approaches to prostaglandin inhibition

   in human disease. Nat Rev Drug Discov. 2, 879-90.

Gregory, A., Westaway, S.K., Holm, I.E., Kotzbauer, P.T., Hogarth, P., Sonek, S.,

   Coryell, J.C., Nguyen, T.M., Nardocci, N., Zorzi, G., Rodriguez, D.,

   Desguerre, I., Bertini, E., Simonati, A., Levinson, B., Dias, C., Barbot, C.,

   Carrilho, I., Santos, M., Malik, I., Gitschier, J., Hayflick, S.J., 2008.

   Neurodegeneration associated with genetic defects in phospholipase A(2).

   Neurology. 71, 1402-9.

Haara, O., Fujimori, S., Schmidt-Ullrich, R., Hartmann, C., Thesleff, I., Mikkola,

   M.L., 2011. Ectodysplasin and Wnt pathways are required for salivary gland

   branching morphogenesis. Development. 138, 2681-91.

Han, C., Lim, K., Xu, L., Li, G., Wu, T., 2008. Regulation of Wnt/beta-catenin

   pathway by cPLA2alpha and PPARdelta. J Cell Biochem. 105, 534-45.

Hatzfeld, M., 1999. The armadillo family of structural proteins. Int Rev Cytol. 186,

   179-224.

Henneke, M., Combes, P., Diekmann, S., Bertini, E., Brockmann, K., Burlina, A.P.,

   Kaiser, J., Ohlenbusch, A., Plecko, B., Rodriguez, D., Boespflug-Tanguy, O.,

Gartner, J., 2008. GJA12 mutations are a rare cause of Pelizaeus-Merzbacher-like disease. Neurology. 70, 748-54.

Henneke, M., Diekmann, S., Ohlenbusch, A., Kaiser, J., Engelbrecht, V., Kohlschutter, A., Kratzner, R., Madruga-Garrido, M., Mayer, M., Opitz, L., Rodriguez, D., Ruschendorf, F., Schumacher, J., Thiele, H., Thoms, S., Steinfeld, R., Nurnberg, P., Gartner, J., 2009. RNASET2-deficient cystic leukoencephalopathy resembles congenital cytomegalovirus brain infection. Nat Genet. 41, 773-5.

Jin, D., Ni, T.T., Sun, J., Wan, H., Amack, J.D., Yu, G., Fleming, J., Chiang, C., Li, W., Papierniak, A., Cheepala, S., Conseil, G., Cole, S.P., Zhou, B., Drummond, I.A., Schuetz, J.D., Malicki, J., Zhong, T.P., 2014. Prostaglandin signalling regulates ciliogenesis by modulating intraflagellar transport. Nat Cell Biol. 16, 841-51.

Joksimovic, M., Awatramani, R., 2014. Wnt/beta-catenin signaling in midbrain dopaminergic neuron specification and neurogenesis. J Mol Cell Biol. 6, 27-33.

Khateeb, S., Flusser, H., Ofir, R., Shelef, I., Narkis, G., Vardi, G., Shorer, Z., Levy, R., Galil, A., Elbedour, K., Birk, O.S., 2006. PLA2G6 mutation underlies infantile neuroaxonal dystrophy. Am J Hum Genet. 79, 942-8.

Lamari, F., Mochel, F., Sedel, F., Saudubray, J.M., 2013. Disorders of phospholipids, sphingolipids and fatty acids biosynthesis: toward a new category of inherited metabolic diseases. J Inherit Metab Dis. 36, 411-25.

Lee, L.Y., Farooqui, A.A., Dawe, G.S., Burgunder, J.M., Ong, W.Y., 2009. Role of phospholipase A(2) in prepulse inhibition of the auditory startle reflex in rats. Neurosci Lett. 453, 6-8.

Li, X., Okada, Y., Pilbeam, C.C., Lorenzo, J.A., Kennedy, C.R., Breyer, R.M., Raisz, L.G., 2000. Knockout of the murine prostaglandin EP2 receptor impairs osteoclastogenesis in vitro. Endocrinology. 141, 2054-61.

Loureiro, J., Peifer, M., 1998. Roles of Armadillo, a Drosophila catenin, during central nervous system development. Curr Biol. 8, 622-32.

Magen, D., Georgopoulos, C., Bross, P., Ang, D., Segev, Y., Goldsher, D., Nemirovski, A., Shahar, E., Ravid, S., Luder, A., Heno, B., Gershoni-Baruch, R., Skorecki, K., Mandel, H., 2008. Mitochondrial hsp60 chaperonopathy causes an autosomal-recessive neurodegenerative disorder linked to brain hypomyelination and leukodystrophy. Am J Hum Genet. 83, 30-42.

Mertin, J., Stackpoole, A., 1978. Suppression by essential fatty acids of experimental allergic encephalomyelitis is abolished by indomethacin. Prostaglandins Med. 1, 283-91.

Milatovic, D., Montine, T.J., Aschner, M., 2011. Prostanoid signaling: dual role for prostaglandin E2 in neurotoxicity. Neurotoxicology. 32, 312-9.

Mohri, I., Taniike, M., Taniguchi, H., Kanekiyo, T., Aritake, K., Inui, T., Fukumoto, N., Eguchi, N., Kushi, A., Sasai, H., Kanaoka, Y., Ozono, K., Narumiya, S., Suzuki, K., Urade, Y., 2006. Prostaglandin D2-mediated microglia/astrocyte interaction enhances astrogliosis and demyelination in twitcher. J Neurosci. 26, 4383-93.

Mullally, J.E., Chernova, T., Wilkinson, K.D., 2006. Doa1 is a Cdc48 adapter that possesses a novel ubiquitin binding domain. Mol Cell Biol. 26, 822-30.

Nakatani, Y., Hokonohara, Y., Kakuta, S., Sudo, K., Iwakura, Y., Kudo, I., 2007. Knockout mice lacking cPGES/p23, a constitutively expressed PGE2 synthetic enzyme, are peri-natally lethal. Biochem Biophys Res Commun. 362, 387-92.

Nguyen, M., Camenisch, T., Snouwaert, J.N., Hicks, E., Coffman, T.M., Anderson,

P.A., Malouf, N.N., Koller, B.H., 1997. The prostaglandin receptor EP4

triggers remodelling of the cardiovascular system at birth. Nature. 390, 78-81.

Nissim, S., Sherwood, R.I., Wucherpfennig, J., Saunders, D., Harris, J.M., Esain, V.,

Carroll, K.J., Frechette, G.M., Kim, A.J., Hwang, K.L., Cutting, C.C., Elledge,

S., North, T.E., Goessling, W., 2014. Prostaglandin E2 regulates liver versus

pancreas cell-fate decisions and endodermal outgrowth. Dev Cell. 28, 423-37.

Palisano, R., Rosenbaum, P., Walter, S., Russell, D., Wood, E., Galuppi, B., 1997.

Development and reliability of a system to classify gross motor function in

children with cerebral palsy. Dev Med Child Neurol. 39, 214-23.

Palumbo, S., Toscano, C.D., Parente, L., Weigert, R., Bosetti, F., 2011. Time-

dependent changes in the brain arachidonic acid cascade during cuprizone-

induced demyelination and remyelination. Prostaglandins Leukot Essent Fatty

Acids. 85, 29-35.

Pusch, C., Hustert, E., Pfeifer, D., Sudbeck, P., Kist, R., Roe, B., Wang, Z., Balling,

R., Blin, N., Scherer, G., 1998. The SOX10/Sox10 gene from human and

mouse: sequence, expression, and transactivation by the encoded HMG

domain transcription factor. Hum Genet. 103, 115-23.

Qiu, L., Pashkova, N., Walker, J.R., Winistorfer, S., Allali-Hassani, A., Akutsu, M.,

Piper, R., Dhe-Paganon, S., 2010. Structure and function of the PLAA/Ufd3-

p97/Cdc48 complex. J Biol Chem. 285, 365-72.

Ribardo, D.A., Peterson, J.W., Chopra, A.K., 2002. Phospholipase A2-activating

protein--an important regulatory molecule in modulating cyclooxygenase-2

and tumor necrosis factor production during inflammation. Indian J Exp Biol.

40, 129-38.

Ruprecht, K., Warmuth-Metz, M., Waespe, W., Gold, R., 2002. Symptomatic hyperekplexia in a patient with multiple sclerosis. Neurology. 58, 503-4.

Schmitz, M., Hermann, P., Oikonomou, P., Stoeck, K., Ebert, E., Poliakova, T., Schmidt, C., Llorens, F., Zafar, S., Zerr, I., 2015. Cytokine profiles and the role of cellular prion protein in patients with vascular dementia and vascular encephalopathy. Neurobiol Aging. 36, 2597-606.

Sievers, F., Wilm, A., Dineen, D., Gibson, T.J., Karplus, K., Li, W., Lopez, R., McWilliam, H., Remmert, M., Soding, J., Thompson, J.D., Higgins, D.G., 2011. Fast, scalable generation of high-quality protein multiple sequence alignments using Clustal Omega. Mol Syst Biol. 7, 539.

Tazir, M., Nouioua, S., Magy, L., Huehne, K., Assami, S., Urtizberea, A., Grid, D., Hamadouche, T., Rautenstrauss, B., Vallat, J.M., 2009. Phenotypic variability in giant axonal neuropathy. Neuromuscul Disord. 19, 270-4.

Teer, J.K., Bonnycastle, L.L., Chines, P.S., Hansen, N.F., Aoyama, N., Swift, A.J., Abaan, H.O., Albert, T.J., Margulies, E.H., Green, E.D., Collins, F.S., Mullikin, J.C., Biesecker, L.G., 2010. Systematic comparison of three genomic enrichment methods for massively parallel DNA sequencing. Genome Res. 20, 1420-31.

Teer, J.K., Green, E.D., Mullikin, J.C., Biesecker, L.G., 2012. VarSifter: visualizing and analyzing exome-scale sequence variation data on a desktop computer. Bioinformatics. 28, 599-600.

Timmons, M., Tsokos, M., Asab, M.A., Seminara, S.B., Zirzow, G.C., Kaneski, C.R., Heiss, J.D., van der Knaap, M.S., Vanier, M.T., Schiffmann, R., Wong, K., 2006. Peripheral and central hypomyelination with hypogonadotropic hypogonadism and hypodontia. Neurology. 67, 2066-9.

Toribio, R.E., Brown, H.A., Novince, C.M., Marlow, B., Hernon, K., Lanigan, L.G., Hildreth, B.E., 3rd, Werbeck, J.L., Shu, S.T., Lorch, G., Carlton, M., Foley, J., Boyaka, P., McCauley, L.K., Rosol, T.J., 2010. The midregion, nuclear localization sequence, and C terminus of PTHrP regulate skeletal development, hematopoiesis, and survival in mice. FASEB J. 24, 1947-57.

Uhlenberg, B., Schuelke, M., Ruschendorf, F., Ruf, N., Kaindl, A.M., Henneke, M., Thiele, H., Stoltenburg-Didinger, G., Aksu, F., Topaloglu, H., Nurnberg, P., Hubner, C., Weschke, B., Gartner, J., 2004. Mutations in the gene encoding gap junction protein alpha 12 (connexin 46.6) cause Pelizaeus-Merzbacher-like disease. Am J Hum Genet. 75, 251-60.

van der Knaap, M.S., Barth, P.G., Stroink, H., van Nieuwenhuizen, O., Arts, W.F., Hoogenraad, F., Valk, J., 1995. Leukoencephalopathy with swelling and a discrepantly mild clinical course in eight children. Ann Neurol. 37, 324-34.

van der Knaap, M.S., 2001. Magnetic resonance in childhood white-matter disorders. Dev Med Child Neurol. 43, 705-12.

Weidenheim, K.M., Dickson, D.W., Rapin, I., 2009. Neuropathology of Cockayne syndrome: Evidence for impaired development, premature aging, and neurodegeneration. Mech Ageing Dev. 130, 619-36.

Yu, Y., Fan, J., Chen, X.S., Wang, D., Klein-Szanto, A.J., Campbell, R.L., FitzGerald, G.A., Funk, C.D., 2006. Genetic model of selective COX2 inhibition reveals novel heterodimer signaling. Nat Med. 12, 699-704.

Zhang, F., Sha, J., Wood, T.G., Galindo, C.L., Garner, H.R., Burkart, M.F., Suarez, G., Sierra, J.C., Agar, S.L., Peterson, J.W., Chopra, A.K., 2008. Alteration in the activation state of new inflammation-associated targets by phospholipase A2-activating protein (PLAA). Cell Signal. 20, 844-61.

Zhang, S., Li, J., Lea, R., Vleminckx, K., Amaya, E., 2014. Fezf2 promotes neuronal

differentiation through localised activation of Wnt/beta-catenin signalling

during forebrain development. Development. 141, 4794-805.

Zivony-Elboum, Y., Westbroek, W., Kfir, N., Savitzki, D., Shoval, Y., Bloom, A.,

Rod, R., Khayat, M., Gross, B., Samri, W., Cohen, H., Sonkin, V., Freidman,

T., Geiger, D., Fattal-Valevski, A., Anikster, Y., Waters, A.M., Kleta, R.,

Falik-Zaccai, T.C., 2012. A founder mutation in Vps37A causes autosomal

recessive complex hereditary spastic paraparesis. J Med Genet. 49, 462-72.

Figure 1. Pedigree of the investigated families. A. Family I: 6 affected individuals (filled shapes). B. Family II: containing another affected individual. A high rate of consanguinity and an AR pattern of inheritance are evident. C. Photographs of patient VI5 (pedigree A) illustrating: coarse facial features (a) pectus carinatum, dystonic posturing, rigidity/freezing and shortening of tendons (b, c), and rocker bottom feet (d).
D. Patients' brain MRI. a and b. T1 Brain MRI of patient IV2 (family II), at 1 year of age, shows white matter atrophy. Corpus callosum is complete but thin. c (T2 MRI Imaging) and d (T1 MRI Imaging). Brain MRI of patient VI3 (family I), at 14 years, shows moderate white matter atrophy and severe corpus callosum thinning. e (T2 MRI Imaging) and f (T1 MRI Imaging). Brain MRI of patient V4 (family I), at age 32 years, shows severe general atrophy. The cortex is usually preserved but very thin, corpus callosum is complete but also very thin. The basal ganglia appear normal.
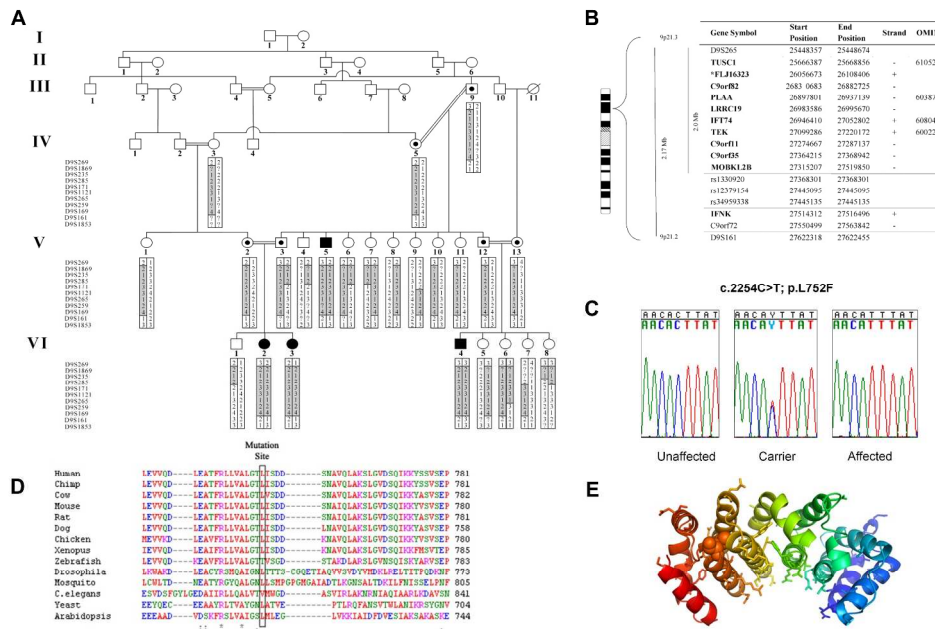
338x190mm (300 x 300 DPI)

Figure 2. A. Haplotypes for each family member were constructed for 11 microsatellite markers spanning the neurodegenerative interval. Markers analyzed are given on the left, according to their physical order. Haplotypes are represented by bars, with the disease-associated haplotype shaded in gray. Reduction in the affected linked region to 1.9Mb was due to healthy individuals VI6 and IV4 who bear fraction of the affected haplotype in a homozygous manner.

B. Physical location of genes and predicted transcripts in the chromosome 9 linked interval. Asterisk denotes genes not approved by the HUGO Gene Nomenclature Committee (HGNC). "Strand" refers to transcription orientation. Bold names indicate gene analyzed by direct sequencing. Physical location obtained from UCSC Human Genome Browser Gateway (hg19 assembly).C. Analysis of the c.2254C>T mutation in exon 14 of PLAA. Sequence analysis is shown for an unaffected individual, an obligatory carrier, and an affected individual. D. Sequence alignment of human PLAA to orthologues in the mutation area. The leucine at position 752 (boxed) in this protein is highly conserved throughout evolution. E. Effect of L752F (Leu→Phe) substitution on PLAA structure. Shown is a ribbon diagram of the PUL domain of PLAA (PDB ID 3EBB) which adopts a banana like shaped Armadillo domain.  The conserved residues of PLAA (homo sapiens, mus musculus, rattus norvegicus, Xenopus laevis, and Saccharomyces cerevisiae) are displayed in stick-representation and form the putative binding site of PLAA.  Mutation of Leu752 shown in ball-representation disrupts the rigid leucine network that tightly holds together the Armadillo domain.
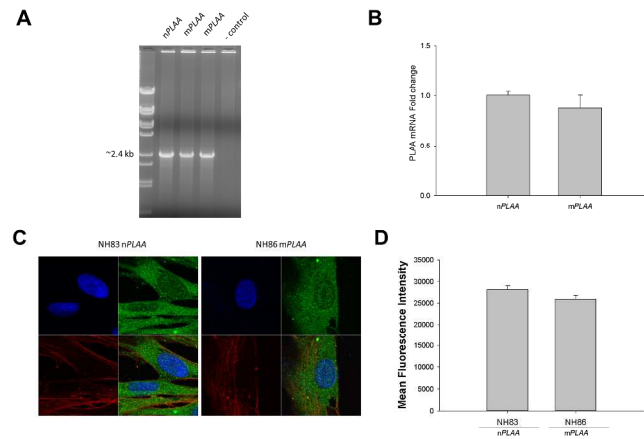
457x304mm (300 x 300 DPI)

Figure 3. mRNA levels for PLAA and confocal microscopy of fibroblasts for the presence of PLAA protein. A. Presence of full length transcript for PLAA from fibroblasts of affected patients and the control subject based on PCR. B. RT-qPCR for the detection of PLAA transcript from fibroblasts of a patient versus the healthy control normalized to four house-keeping genes coding for human 18S RNA, GAPDH, PolB, and L19 ribosomal protein. Arithmetic means ± standard deviations from three biological replicates performed in triplicate were shown. C. Fibroblasts (nPLAA or mPLAA) were counterstained with DAPI (blue) for the nucleus and with fluorophore conjugated phalloidin (red) for actin. Cells were fixed, subjected to immunofluorescence staining for PLAA (green), and observed by confocal microscopy. D. Mean fluorescence intensity of regions of interest corresponding to the cytoplasm and nucleus of imaged cells (Image J processing program, NIH). Figure represents results from 3 sets of images and error bars represent standard deviations.
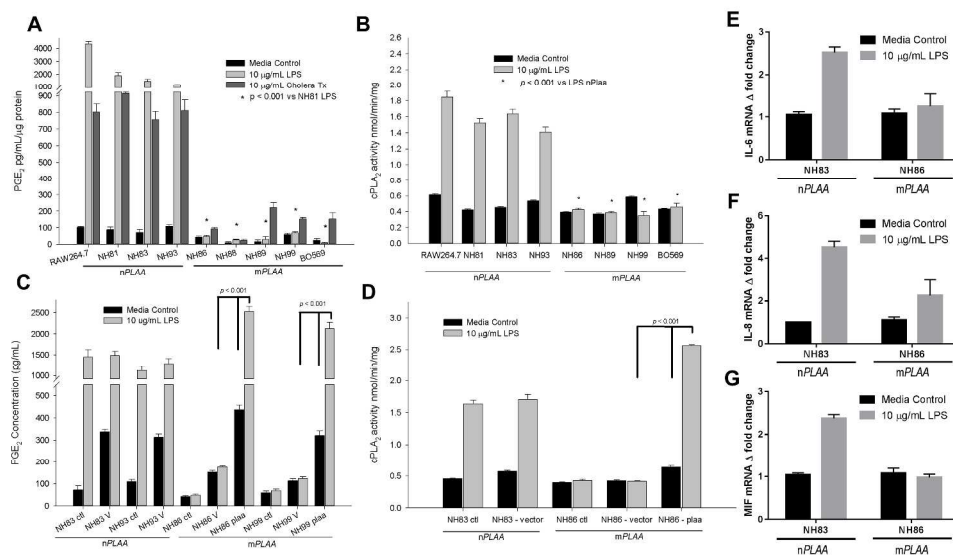
338x190mm (300 x 300 DPI)

Figure 4. PGE2 levels and cPLA2 activity are low in patients' fibroblasts, and could be rescued. A. Levels of PGE2 in cell culture media after 24 hours of stimulation with LPS or cholera toxin Levels of PGE2 were normalized against protein concentrations in the supernatants. All cells were primary human fibroblasts except RAW 264.7 cells which are murine macrophage like cells and used as a positive control. B. Activity of cPLA2 in the membrane fractions of fibroblasts and RAW 264.7 macrophages. Cells were stimulated with or without LPS for 24 hours before harvesting and purification of the membrane fractions. The cPLA2 activity was normalized to amount of proteins added to the assay. C. PGE2 levels in the cell culture media after transfection with CMV promoter-based pIRES2-DsRed2 plasmid containing the native PLAA gene and a fluorescent marker of transfection. Cells were treated as follow: ctl = no transfection; V = transfection with empty vector; PLAA = transfection with plasmid vector containing the wild type PLAA. D. cPLA2 activity from membrane fractions of fibroblasts after transfection with a plasmid containing the nPLAA in a CMV promoter-based vector system and a fluorescent marker of transfection. E-G. Fold changes in transcripts for IL-6, IL-8, and MIF based on RT-qPCR. Arithmetic means ± standard deviations from three independent experiments performed in triplicate were plotted and the data were analyzed using one way ANOVA with Tukey post-hoc correction.
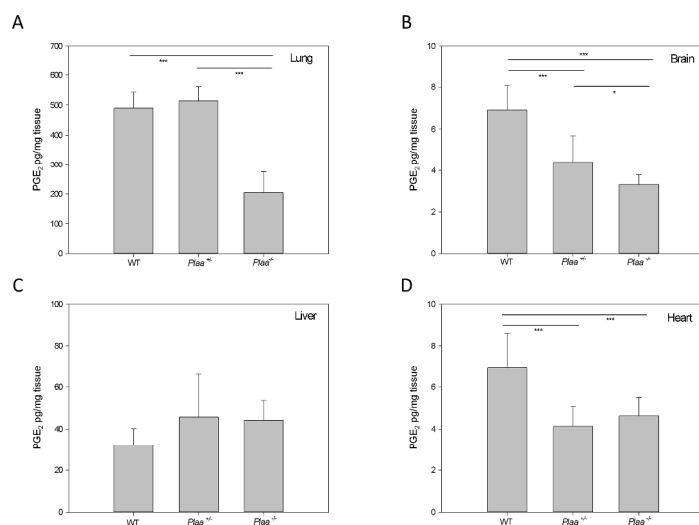
338x190mm (300 x 300 DPI)

Figure 5. PGE2 levels in embryonic mouse tissues. WT, Plaa+/-, and Plaa-/- embryos were sacrificed at E18.5 and organs were isolated and prostaglandin levels determined for the lung (A), brain (B), liver (C), and heart (D). Data represented arithmetic means ± standard deviations from tissues representing 3 WT, 3 Plaa+/-, and 4 Plaa-/- embryos and obtained from three independent littermates. Significance was determined by one way ANOVA with Tukey post-hoc correction. * denotes p<0.05   *** denotes p<0.001.
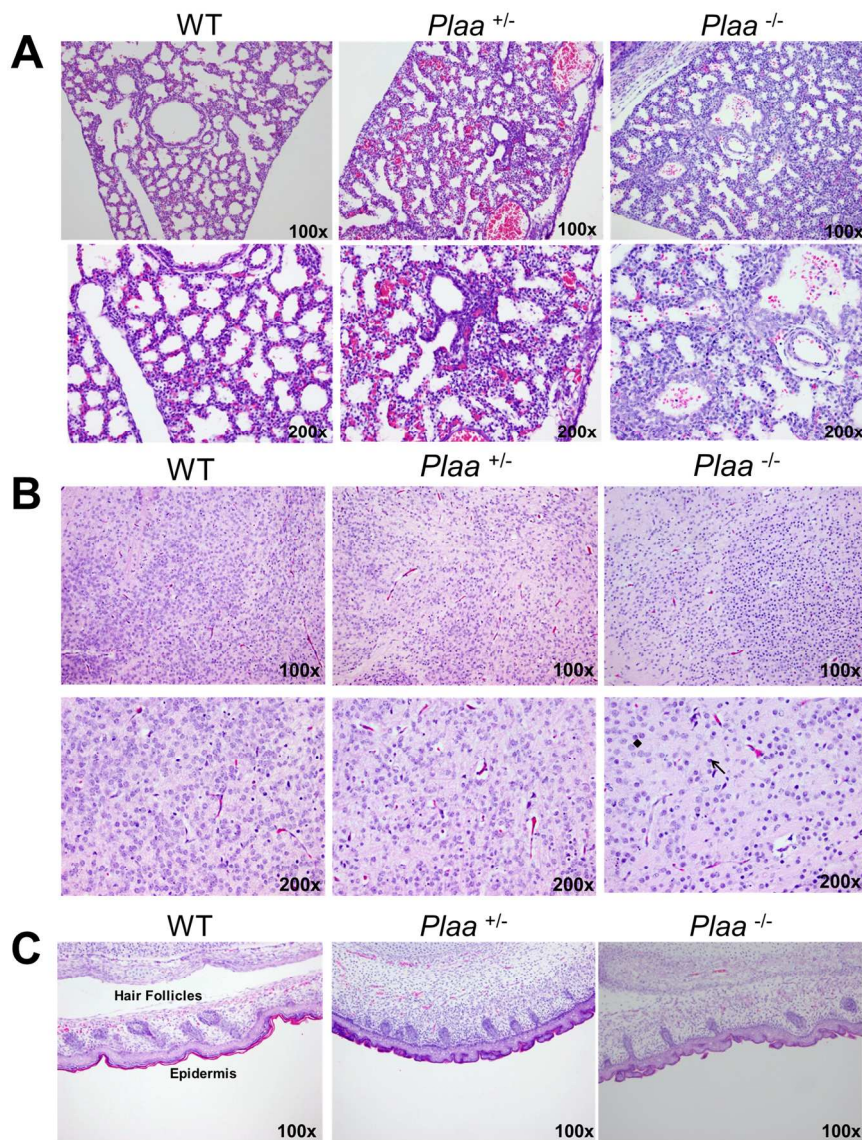
338x190mm (300 x 300 DPI)

Figure 6. Histopathology of embryonic mouse tissues. Lungs (A), brain cerebral cortex (B), and skin (C) were H&E stained and analyzed in a blinded fashion.  Tissues representing 2 WT, 2 Plaa+/-, and 4 Plaa-/- embryos were analyzed. Multiple fields for each tissue were visualized and typical representations are shown with magnifications.

152x190mm (300 x 300 DPI)

*Supplementary Materials and Methods*

## Western blot analysis

*Ubiquitin.* Western blotting was performed with a SDS-PAGE Electrophoresis System as described previously (Khayat *et al.*, 2008). Briefly, 30 μg protein samples from healthy controls' and patients' fibroblasts were prepared in a reducing sample buffer, and then electrophoresed on a 7.5% Tris gel with Tris running buffer; blotted to nitrocellulose membrane; and probed with mouse anti-ubiquitin (Santa Cruz Biotechnology, Inc., Santa Cruz, CA) antibodies. A horseradish peroxidase-conjugated goat anti-mouse secondary antibody (Santa Cruz) was then added, and proteins detected by autoradiography using enhanced chemiluminescence substrate (Pierce ECL kit, Thermo Scientific, Grand Island, NY).

## Yeast experiments

Wild type *DOA1* gene expressing plasmid and *DOA1* deleted yeast strain (*Saccharomyces cerevisiae*) were kindly provided by Prof. Tzachi Pilpel and Dr. Orna Dahan (Weizmann Institute of Science, Israel). Mutant p.Leu677Phe (Leucine→ Phenylalanine) *DOA1* was produced using the Quikchange site-directed Wild type or mutant *DOA1* expressing plasmid, or a mock plasmid, was transformed into the indicated yeast strain by standard lithium acetate method. The yeast was grown on a regular synthetic medium at 30°C, 37°C or at 30°C supplemented with 0.5 μg/ml cycloheximide. After three days, the growth of the yeast was assessed.

## Cell biology studies

*Immunofluorescence Confocal Microscopy*

Confocal microscopy was performed on fixed fibroblasts by established procedures with slight modifications. Briefly, nPLAA and mPLAA were treated with 10 μg/mL LPS for 60 min, with LPS untreated cells serving as controls, before fixation with 4% paraformaldehyde. Subsequently, fibroblasts were permeabilized with 0.5% Triton X-100. Goat anti-p65 C-20 antibody (Santa Cruz) or rabbit anti-PLAA antibody (GenWay Biotech, Inc., San Diego, CA), and Alexa Fluor 488 donkey anti-goat antibody (Molecular Probes, Carlsbad, CA) or Alexa Fluor 488 donkey anti-rabbit antibody, were used as primary and secondary antibodies, respectively, as appropriate. Samples stained with secondary antibody alone were used as negative controls. Fibroblasts were then counterstained with DAPI (Life Technologies, Grand Island, NY) and Alexa Fluor 594 phalloidin (Life Technologies) to stain the nucleus and actin, respectively. Fibroblasts were subsequently visualized using a Zeiss LSM510 confocal scanning microscope.

*Plaa Gene Targeting*

A mouse genomic library, ES129SvJ, was screened for clones containing the *Plaa* gene. Two overlapping pUC18 clones, 10-1-1A carrying a ~17-kb *Plaa* upstream-intron 2 region and 7-2-1A carrying a ~12-kb *Plaa* intron 2-intron 10 region, were validated for the organization of the gene by DNA restriction enzyme digestion and sequence analysis, and used for knockout vector construction. A 3.1-kb *Hin*dIII-*Bgl*II fragment (intron 1, 5' homology arm), and a 6.0-kb *Sal*I-*Asp*718 (located in pUC18) fragment containing exons 8-10 (3' homology arm) were subcloned into a plasmid vector, pBluescript II KS (-) (Agilent Technologies). A positive selection marker PGK*neobpA* (Soriano *et al.*, 1991) flanked by *loxP* sites was inserted between two homology arms, and a negative selection marker HSV*tkpA* (Mansour *et al.*, 1988) was inserted between pBluescript and the 5' homology arm (**Figure S2, A**).

The vector was linearized at the end of the 3' homology arm by *Asp*718 and

electroporated into 129S inbred Tc1 (George et al., 2007)kindly provided by Phillip

Leder, Harvard Medical School, Boston, MA) and B6129F$_1$ hybrid G4 (George et al.,

2007) kindly provided by Andras Nagy, Samuel Lunenfeld Research Institute, Mount

Sinai Hospital, NY) mouse embryonic stem (ES) cells.

A 3'-flanking probe was used in Southern blot for the identification of targeted clones

(**Figure S2, A**). Mutant ES cell clones were injected into C57BL/6J blastocysts. We

crossed chimeric mice and C57BL/6J to produce animals heterozygous for the *Plaa*

knockout (KO)$^{neo}$ allele. To establish mutant lines with *Plaa* exon-2-7 deletion (KO)

allele, we crossed KO$^{neo}$/+ mice to a germ-line *cre* deleter strain, Zp3-cre transgenic

mouse, on a C57BL/6J background (Lewandoski et al., 1997)C57BL/6J-Tg(Zp3-

*cre*)93Knw/J, The Jackson Laboratory, Stock Number: 003651). The mice were

maintained by backcrossing to C57BL/6J.

*Genotyping*

We genotyped mice initially by Southern blot analysis using the 3' probe, and

subsequently by PCR (**Figure S2, B&C**). The 3' probe was generated by PCR with

primers: XB-X-*Plaa*, 5'-CTTCTCGAGTTCCTGAATGTCTGGGAAAA-3'; and

XB-B-*Plaa*, 5'-ACGAGATCTAGTGATGTGGCAATGCCTTT-3'; and mouse

genomic DNA as the template. The PCR product was treated with Klenow DNA

polymerase, digested with *Bgl*II, and subcloned into pBluescript II SK (-) at *Eco*RV

and *Bam*HI sites (p*Plaa* 3' XB). The digestion of the plasmid p*Plaa* 3' XB by *Xho*I

and *Xba*I restriction enzymes released a ~450-bp DNA fragment corresponding to

*Plaa* exon 13 and its flanking region. Genotyping PCR was performed with the

following primers: PlaaWTF, 5'-GGGGGTGGCGTTCCATGTGT-3'; PlaaM+F, 5'-

GTGGGGCAGGACAGCAAG-3'; PlaaM-F, 5'-CCATTTGGCTTTTTGGTCTT-3';

and PlaaCMR, 5'-CCACCTCCCGTCACTAACACTCCA-3'. PCR conditions for the

genotyping will be provided upon request.

Supplementary Results

*Functional Effects of p.Leu752Phe on* PLAA

While the ΔDOA1 strain displayed abrogated growth, transformation of the ΔDOA1

strain with a plasmid expressing either the native *DOA1* gene or its p.Leu677Phe

variant, which corresponds to Leu752 in human PLAA, completely rescued the

growth phenotype of *S. cerevisiae* ΔDOA1 mutant strain (data not shown). Likewise,

we found no evidence of effect of p.Leu752Phe variation of PLAA on ubiquitin

depletion in fibroblasts from healthy controls versus patients based on Western blot

analysis (data not shown).

 *NF-κB Recruitment to the Nucleus is Unaffected by p.Leu752Phe in the PLAA.*

As the secretion of PGE$_2$ as well as the activity of cPLA$_2$ was decreased in m*PLAA*

fibroblasts, we investigated whether NF-κB signaling was intact. We stimulated

n*PLAA* and m*PLAA* cells with 10 μg/mL LPS for 60 min and compared nuclear

localization of p65 by confocal microscopy. Unstimulated n*PLAA* and m*PLAA*

fibroblasts exhibited comparable fluorescent staining primarily in the cytoplasm with

little to no nuclear staining (**Figure S1**A,B). Upon stimulation with LPS, both n*PLAA*

and m*PLAA* fibroblasts showed localized NF-κB staining primarily in the nucleus,

with no significant differences between cell types (n*PLAA* versus m*PLAA* fibroblasts).

These data suggested that the NF-κB signaling pathway remained intact and that

differences in phenotype observed for m*PLAA* fibroblasts could be localized

downstream of NF-κB signaling.

*Wnt Signaling is Not Affected by p.Leu752Phe* PLAA

β-catenin mediated wingless integration (Wnt) signaling has been shown to play an important role in early embryonic development, neurogenesis, central nervous system morphogenesis, hirsutism, sweat gland morphology, short tendons, and kyphosis (Haara et al., 2011 ; Joksimovic and Awatramani, 2014; Toribio et al., 2010; Zhang et al., 2014).(Chenn, 2008). Han and collegues have shown this pathway to be regulated by cPLA2a (Han et al., 2008). Therefore, we investigated Wnt signaling by examining levels of non-phospho (active) β-catenin in n*PLAA* versus m*PLAA* fibroblasts with and without LPS stimulation. As shown in **Figure S1C**, the levels of active β-catenin were increased after LPS stimulation to a similar extent in both types of fibroblasts. These data indicated that the variant *PLAA* in our patients did not alter canonical Wnt signaling pathway.

*Supplementary Figure Legends*

**Figure S1. Evaluation of NF-κB translocation and Wnt signaling**. **A.** Samples (see legends for Figure 4) were counterstained with DAPI (blue) for the nucleus and with fluorophore conjugated phalloidin (red) for actin. Cells were stimulated with or without LPS for 1 h, then fixed and subjected to immunofluorescence staining for p65 of NF-κB (green). **B.** Mean fluorescence intensity of regions of interest (Image J processing program) corresponding to the nucleus and cytoplasm of cells stimulated with and without LPS is shown. Figure represents results from 3 sets of images and error bars indicate standard deviations. **C.** The whole cell lysates from n*PLAA* and m*PLAA* fibroblasts with and without LPS treatment were subjected to Western blot analysis and probed with non-phospho (active) β-catenin antibodies. Antibodies to β-tubulin were used as a loading control. Three independent experiments were performed and fold changes in the level of β-catenin (based on densitometer scanning of the bands) and normalized to the internal control with and without LPS treatment are shown.

**Figure S2. *Plaa* gene targeting.** We replaced an exon-2-7 region of the mouse *Plaa* gene with a *neo* cassette flanked by *loxP* sites.  The cassette was subsequently removed *via cre-loxP* recombination. The *Plaa* mutant allele with *neo* cassette and the one without the cassette resulted in the same phenotype. **A.** Maps of the *Plaa* wild-type (WT) allele, knockout (KO) vector, KO$^{neo}$ allele, and KO allele. Exons 1-14 are shown as boxes. Blue, pink, yellow, and red triangles indicate genotyping primers: PlaaWT, PlaaM+F, PlaaM-F, and PlaaCMR, respectively. A, *Asp*718; BI, *Bgl*I; BII, *Bgl*II; H, *Hin*dIII; and S, *Sal*I. **B.** Southern blot analysis of genomic DNA isolated from three *Plaa*-KO$^{neo}$/+ mouse embryonic stem cell clones and a random integration clone (R). The 3' flanking probe hybridized to a 22.6-kb *Bgl*I DNA fragment from

WT allele, and a 14.7-kb *Bgl*I DNA fragment from KO^{neo} allele. The *neo* probe also

hybridized to the 14.7-kb *Bgl*I DNA fragment. We identified three ES cell clones that

incoorporated the *Plaa* mutation by Southern blot analysis. The clones #27 and 75

were derived from Tc1 ES cells; the clone #52 was derived from G4 ES cells. The

clones #27 and 52 transmitted the mutant allele to the germ line of the mouse.  **C.**

PCR genotyping of the mouse. The upper panel shows genotyping results for E14.5

embryos produced by *Plaa*-KO^{neo} heterozygous intercrosses; the lower panel shows

genotyping results for *Plaa*-KO lines.

References

Chenn, A., 2008. Wnt/beta-catenin signaling in cerebral cortical development.
Organogenesis. 4**,** 76-80.

George, S.H., Gertsenstein, M., Vintersten, K., Korets-Smith, E., Murphy, J., Stevens,
M.E., Haigh, J.J., Nagy, A., 2007. Developmental and adult phenotyping
directly from mutant embryonic stem cells. Proc Natl Acad Sci U S A. 104**,**
4455-60.

Haara, O., Fujimori, S., Schmidt-Ullrich, R., Hartmann, C., Thesleff, I., Mikkola,
M.L., 2011. Ectodysplasin and Wnt pathways are required for salivary gland
branching morphogenesis. Development. 138**,** 2681-91.

Han, C., Lim, K., Xu, L., Li, G., Wu, T., 2008. Regulation of Wnt/beta-catenin
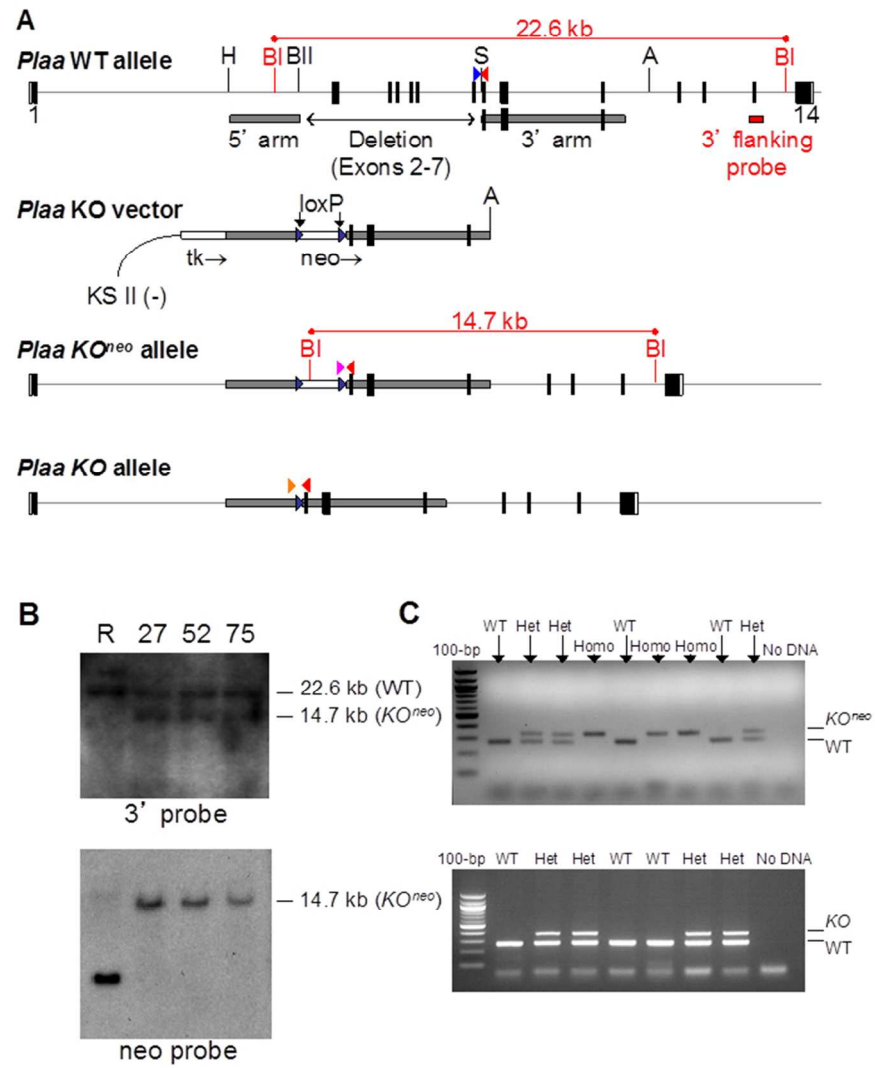pathway by cPLA2alpha and PPARdelta. J Cell Biochem. 105**,** 534-45.

Joksimovic, M., Awatramani, R., 2014. Wnt/beta-catenin signaling in midbrain

dopaminergic neuron specification and neurogenesis. J Mol Cell Biol. 6**,** 27-

33.

Khayat, M., Korman, S.H., Frankel, P., Weintraub, Z., Hershckowitz, S., Sheffer,

V.F., Ben Elisha, M., Wevers, R.A., Falik-Zaccai, T.C., 2008. PNPO

deficiency: an under diagnosed inborn error of pyridoxine metabolism. Mol

Genet Metab. 94**,** 431-4.

Lewandoski, M., Wassarman, K.M., Martin, G.R., 1997. Zp3-cre, a transgenic mouse

line for the activation or inactivation of loxP-flanked target genes specifically

in the female germ line. Curr Biol. 7**,** 148-51.

Mansour, S.L., Thomas, K.R., Capecchi, M.R., 1988. Disruption of the proto-

oncogene int-2 in mouse embryo-derived stem cells: a general strategy for

targeting mutations to non-selectable genes. Nature. 336**,** 348-52.

Soriano, P., Montgomery, C., Geske, R., Bradley, A., 1991. Targeted disruption of the

c-src proto-oncogene leads to osteopetrosis in mice. Cell. 64**,** 693-702.

Toribio, R.E., Brown, H.A., Novince, C.M., Marlow, B., Hernon, K., Lanigan, L.G.,

Hildreth, B.E., 3rd, Werbeck, J.L., Shu, S.T., Lorch, G., Carlton, M., Foley, J.,

Boyaka, P., McCauley, L.K., Rosol, T.J., 2010. The midregion, nuclear

localization sequence, and C terminus of PTHrP regulate skeletal

development, hematopoiesis, and survival in mice. FASEB J. 24**,** 1947-57.

Zhang, S., Li, J., Lea, R., Vleminckx, K., Amaya, E., 2014. Fezf2 promotes neuronal

differentiation through localised activation of Wnt/beta-catenin signalling

during forebrain development. Development. 141**,** 4794-805.
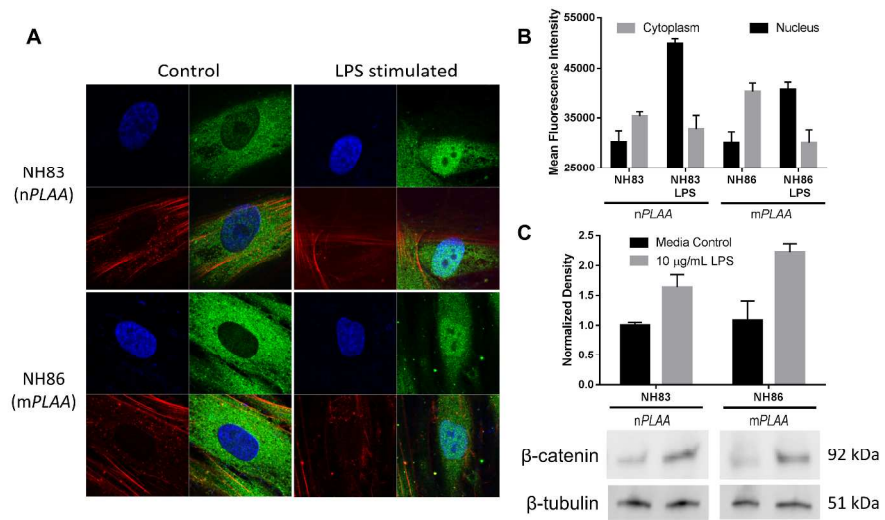
338x190mm (300 x 300 DPI)

Figure S2



190x254mm (96 x 96 DPI)